Master thesis
Sustainable Process Technology

Heat transfer to sub- and supercritical water flow in a vertical tube at low mass fluxes

Wilmar den Hartog
s1004271
January 2016

Committee:
Prof.dr. S.R.A. Kersten
Dr.ir. A.G.J. van der Ham
Dr. M.A. van der Hoef
Dr.ir. D.W.F. Brilman
S.O. Odu, MSc

UNIVERSITEIT TWENTE.

Abstract

Within the Sustainable Process Technology research group of the University of Twente several processes are investigated which are operated at supercritical water conditions (T>374.0°C and P>22.05 MPa [1]). For example, supercritical water desalination, supercritical water gasification both operating at low mass fluxes [2]. Operating processes at these conditions is highly energy consuming and has direct influence on the operating costs. Therefore heat integration is essential in these processes. Literature [4] describes a lot of research about heat transfer at sub- and supercritical water at high mass fluxes (G>200 kg/m^2s [4]) and in a turbulent flow regime. In previous research [5; 6] a correlation for the heat transfer coefficient is developed for low mass fluxes (G<20 kg/m^2s) in the (overall) laminar flow regime. This correlation is supported with experimental results at subcritical temperatures.

In this research experiments were carried out in a vertical tube (OD of 33.40 mm, ID of 20.70 mm and length of 1.54 m) with upward flow at sub- and supercritical conditions. Experiments were done with 3 different flow rates; 4.1 (G=3.2 kg/m^2s), 8.0 (G=6.3 kg/m^2s) and 11.3 kg/h (G=8.8 kg/m^2s). Temperatures are measured axial direction and in radial direction at a specific position. To get axial and radial temperature profiles. For the radial temperature profile in the fluid a probe with multiple thermocouples is used and for the radial temperature profile in the wall multiple thermocouples where placed in the tube wall at two positions (55 cm and 100 cm from the inlet). With the temperatures results from the wall the heat flux and thi inner wall temperature can be calculated. The temperatures of the probe are used to estimate the fluid temperature. Finally the Heat Transfer Coefficient (HTC) is calculated from the heat flux and temperature difference between the wall and fluid.

The results obtained at 300 bar and 55 cm are the most consistent. Below 350 C the results of the experimental HTC are within the error bar in agreement with the correlation and increase from 1 kW/m^2.°C up to 2 kW/m^2.°C with temperature. However the experimental HTCs are always above the values obtained from the correlation. Above 350°C the HTC increases exponentially up to the pseudocritical temperature, which is not the case for the correlation. Experimental and correlation results show an increasing HTC at an increasing flow rate.

The measurements at 100 cm are more difficult to interpret. Probably as a result of an axial temperature gradient in the wall the radial temperature profile in the wall shows a maximum. Due to this it is impossible to separate the radial and axial heat flux. Estimation of the maximum and minimum radial heat flux is conducted but it results in HTCs, which deviate too much.

Contents

List of Figures

List of Tables

Nomenclature

Symbols

A	heat transfer area	m^2
C_p	specific isobaric heat capacity	kJ/(kg.°C)
D	inside diameter	m
d_i	tube inside diameter	m
d_o	tube outside diameter	m
g	gravitational constant	m/s^2
G	mass flux	$kg/(m^2.s)$
Gr	Grashof number	-
h	enthalpy	kJ/kg
hi	tube-side heat transfer coefficient	$W/(m^2.°C)$
ID	inner diameter	m
k	thermal conductivity	W/(m.°C)
L	heated length	m
m	mass flow rate	kg/s
Nu	Nusselt number	-
OD	outer diameter	m
P	pressure	bar or MPa
Pr	Prandtl number	-
Q	amount of transferred heat	W
R	gas constant	J/(K.mol)
R	tube radius	-
Re	Reynolds number	-
T	temperature	°C
T_c	centre-line temperature (at r=0)	°C
T_{in}	inlet temperature	°C
T_{iw}	inner wall temperature	°C
T_{mc}	mixing cup temperature	°C
T_{ow}	outer wall temperature	°C
U_o	overall heat transfer coefficient	$W/(m^2.°C)$
x	axial coordinate	m

Greek letters

β	thermal expansion coefficient	1/°C
μ	viscosity	Pa.s
ρ	density	kg/m^3
ϕ	flow rate	kg/h

Subscripts

b	bulk
cr	critical
i	thermocouple location in the fluid
iw	inside wall
mc	mixing cup
ph	preheater
s	shell / annulus
w	wall

Abbreviations

BPR	Back Pressure Regulator
HB	Heating Block
HTC	Heat Transfer Coefficient
PI	Pressure Indicator
SCW	Supercritical water
SPT	Sustainable Process Technology
T-C	Temperature Control
T-S	Temperature Safety Control

1 Introduction

This research is a graduation assignment of the master Chemical and Process Engineering at the research group Sustainable Process Technology (SPT) of the University of Twente. In this chapter the background and content of the assignment are described.

1.1 Background

Within the SPT research group several processes are investigated which are operated at supercritical water conditions (T>374.0 °C and P>22.1 MPa [1]). For example, supercritical water desalination, supercritical water gasification [2]. Operating processes at these conditions is highly energy consuming, due to the high amount of energy required to heat the feed stream and the heat loss by cooling the product stream. These have direct influence on the operating costs and therefore the economically feasibility of the process. The operating costs can be reduced to make the process more economic feasible, heat integration is essential in these processes. Heat integration is achieved by heating the feed stream with the product stream in a heat exchanger that operates at supercritical pressure and sub- to supercritical temperatures.

In the critical region, where these processes operate, the properties of water change drastically with small changes in temperature. Change in properties like density, viscosity, heat capacity and thermal conductivity have influence on the heat transfer and therefore also on the design of the heat exchanger [3].

Many heat transfer coefficient (HTC) correlations are available in literature [4] for various fluids, including water, at sub- and supercritical pressures [3]. Pioro and Duffey have performed a preliminary analysis on these HTC correlations and found that the correlation of Bishop et al. was fitting well for sub- to supercritical water flow at high mass fluxes in vertical tubes [4]. The Dittus-Boelter correlation is widely used as heat transfer correlation at subcritical pressures for forced convection [3]. Later on the Dittus-Boelter correlation is adjusted to fit experimental data for heat transfer at supercritical pressures [4]. The correlation of Bishop et al. is also based on the Dittus-Boelter correlations. Morky [3] decribes more researchers who have adjusted or used these correlations, but these researches are mainly in the turbulent flow.

In previous experimental research, on laminar flow, an indirect method is used to calculate the heat transfer coefficient [5]. These indirect method is based on enthalpy difference in the energy balance [5]. In this report a direct method will be used, based on the heat flux measurements through the tube wall. This will be explained in more detail in the chapter 3 (Experimental section).

1.2 Objectives

In previous research on heat transfer to sub- and supercritical water, a HTC correlation was obtained from Comsol simulations [6]. Previous experimental work has been carried out at temperatures below the pseudo-critical point[1], where the HTC is constant. One objective is to measure a maximum value of HTC. This will be done experimentally by crossing the pseudo-critical temperature of water at the operating pressure. The second objective is to study the effect of (supercritical) pressure on HTC at sub- and supercritical temperatures. The expectation of this research is that a higher maximum value of HTC will be obtained when the pressure is closer to the critical pressure of the water. HTCs obtained from experiments will be compared to the predictions of the HTC correlation obtained from Comsol.

1.3 Outline of the thesis

In the following chapter a literature overview is given about properties of supercritical fluids, like water and other solvents. The properties of these fluids will be compared with each other. Here also prediction methods for heat transfer at supercritical pressure are presented. These methods are for turbulent flow of supercritical fluids. The third chapter is about the experimental methods and the calculation procedure. In chapter 4 the results will be discussed and in the succeeding chapters the conclusion and recommendation will be given.

[1] Pseudo-critical point is a point at a pressure above the critical pressure and temperature above the critical temperature corresponding to the maximum value of the specific heat capacity for the particular operating pressure.

2 Literature review

In this chapter the literature review on supercritical water and other solvents is given. The focus will lay on different properties of supercritical fluids and especially the heat transfer coefficient (HTC). Also a literature review of available HTCs correlations for sub- and supercritical water flow in tubes is given.

2.1 Supercritical water (SCW)

A fluid, like water, is supercritical when the temperature and pressure exceed the temperature and pressure at the critical point, see the phase diagrams in Figure 1 [7]. The critical point of a fluid is at the end point of the liquid-vapour equilibrium. Above this point a fluid cannot be liquefied. The fluid is then neither a liquid nor gas but has approximate the behaviour of a perfect gas [4]. After this point the phase boundary vanishes (Figure 1(a) and (b)), but there is a pseudocritical line. Each point on the pseudocritical line have a temperature and pressure above critical temperature and critical pressure which corresponds to the maximum value of the specific heat at the particular pressure [8].

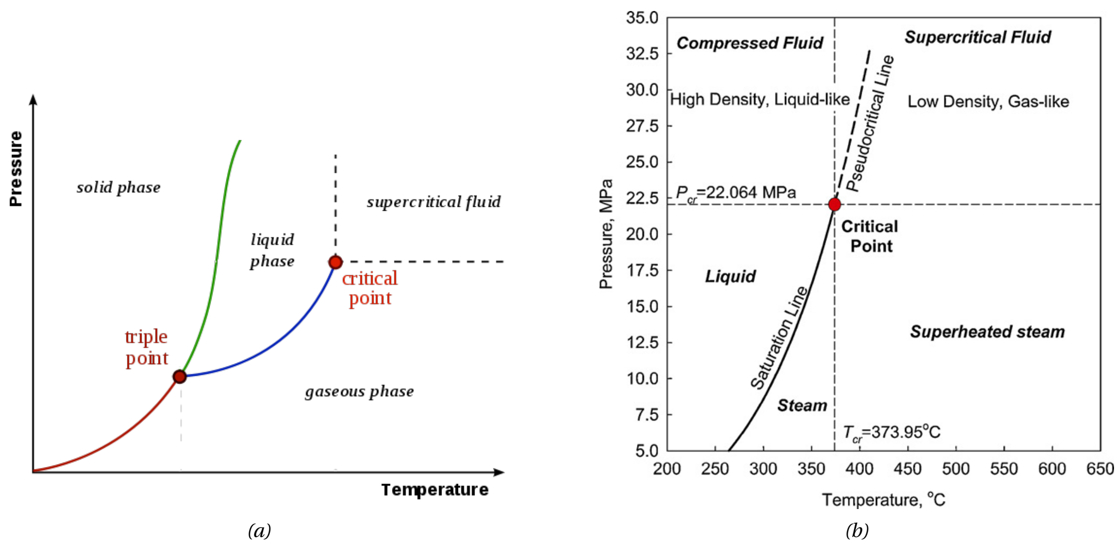

Figure 1: (a): Phase diagram of most substances [9]. (b): Phase diagram of water [8].

The properties of supercritical fluids changes rapidly with small changes in temperature and pressure around the critical point as for water which is shown in Figure 2. Water has an unusually high critical temperature this is due to the high polarity of water [10]. Water has a liquid density of 998.2 kg/m^3 at 20°C [11] and for steam 0.59 kg/m^3 at 100°C [12] both at atmospheric pressure. From Figure 2(a) it can be seen that the densities of supercritical water are lower than liquid water (at 20°C), but higher than steam at atmospheric pressures [7]. In Figure 2 (a)-(c) the red and blue lines of 210 bar and 221 bar are showing a straight vertical line, but for the 221 bar it is less pronounced. The 210 bar is below the critical pressure of 220.5 bar, therefore there is a phase transition over the saturation line from liquid to gas. Change in properties, where the pressure and temperature are slightly higher than the critical point conditions, are large (Figure 2(c)) but near the pseudocritical points, by an increase of pressure, the change of properties are less pronounced [4; 8]. The specific isobaric heat capacity of water near the critical point is 2-9 times higher than of liquid water, which means that supercritical water can absorb more energy per unit of weight per temperature difference than liquid water, see Figure 2(c). Therefore the heat transfer will be better for supercritical water than liquid water.

The properties change of the fluid in the supercritical region have some benefits in the applications in the process industry. So water under supercritical conditions can be used as an extractive agent [1]. The dielectric constant of SCW is much lower than liquid water and the hydrogen bonds become weaker, which make SCW a good agent to dissolve most of the (nonpolar) organic compounds [7; 10]. Also electrolytes with the formation of ions can dissolve in SCW if the density and relative permittivity are sufficiently high [7]. SCW is used to cool nuclear reactors (SCWR) due to the good heat transfer of SCW. Supercritical water nuclear power plants have comparable with a regular nuclear power plants a much higher operating parameters and therefore a simplified flow circuit [4]. This is possible due to the relatively constant density of SCW under supercritical operating conditions, see Figure 2(a). Besides its use as

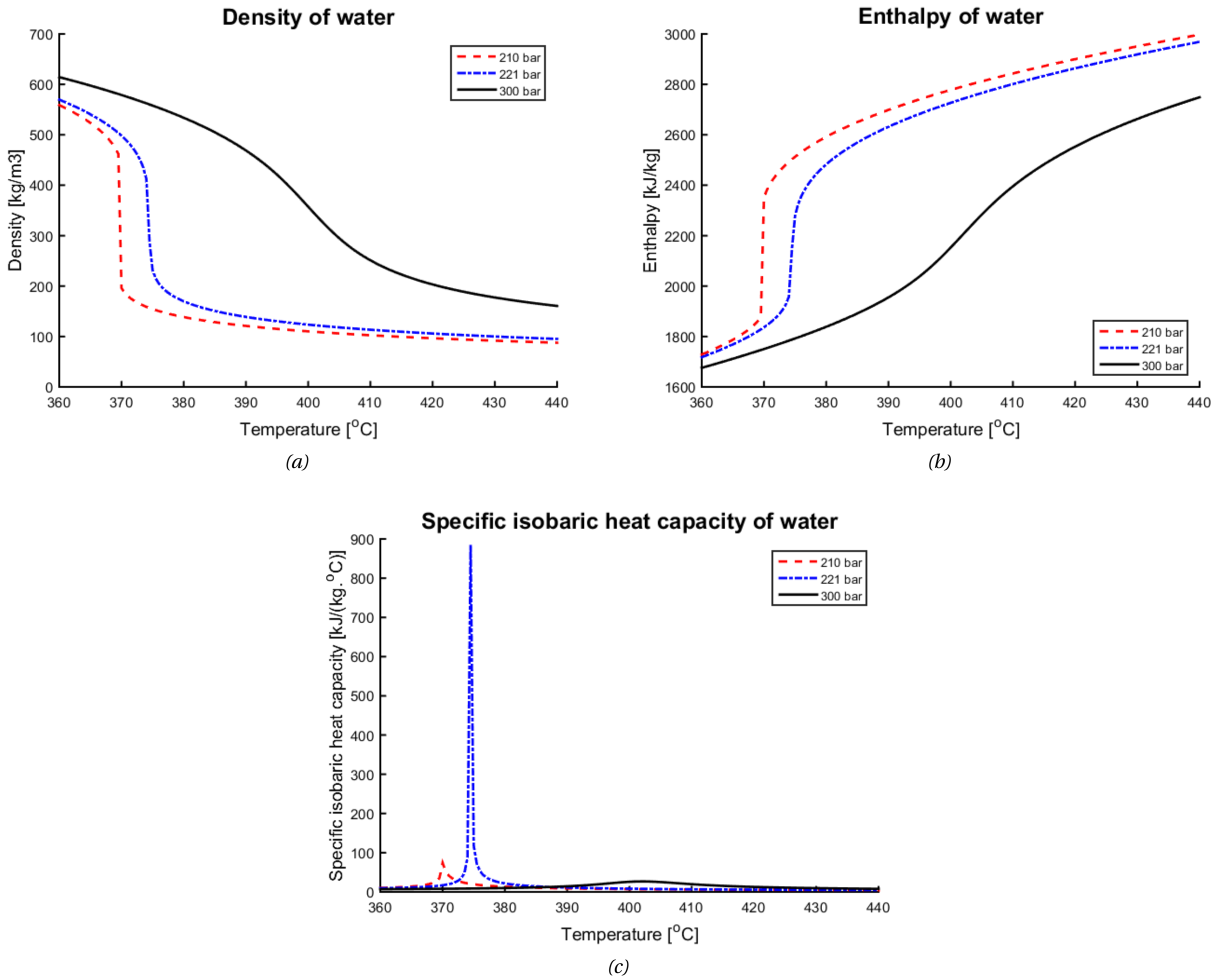

Figure 2: Different properties of water at 210, 222 and 300 bar; (a) Density, (b) Enthalpy and (c) Specific isobaric heat capacity [13].

an extractive agent and coolant, SCW can be used in reactions. If the pressure is high enough SCW is miscible with organic compounds and oxygen, which make it an attractive medium for (hydrothermal) oxidation reactions [10]. The drawbacks of using SCW are the high pressure and high temperature [10].

2.1.1 Heat transfer at SCW conditions

Natural convection

Due to the strong change in properties near the (pseudo-) critical point, a strong buoyancy effect and acceleration effect exist near the wall [14; 6]. Hodes et al. [15] said that when natural convection become important it may reduce or enhance forced convective heat transfer. The importance depends on forced convection, tube orientation, flow direction, and flow regime (turbulent or laminar). So will in laminar, vertical flows, buoyancy forces which act in the flow direction increase the heat transfer, while the buoyancy forces in opposite direction reduce the heat transfer. In case of the turbulent upward flow, natural convection can enhance or reduce the heat transfer [15].

Heat transfer coefficient of sub- and supercritical water

Yamagata et al. [16] found that the HTC increases abruptly when the bulk temperature become close up to the pseudocritical temperature, see Figure 3. Furthermore, they show that the maximum HTC value increases with a decrease of the heat flux.

Yamagata et al. [16] concluded from his experiments that there is no appreciable difference in HTC for the flows in

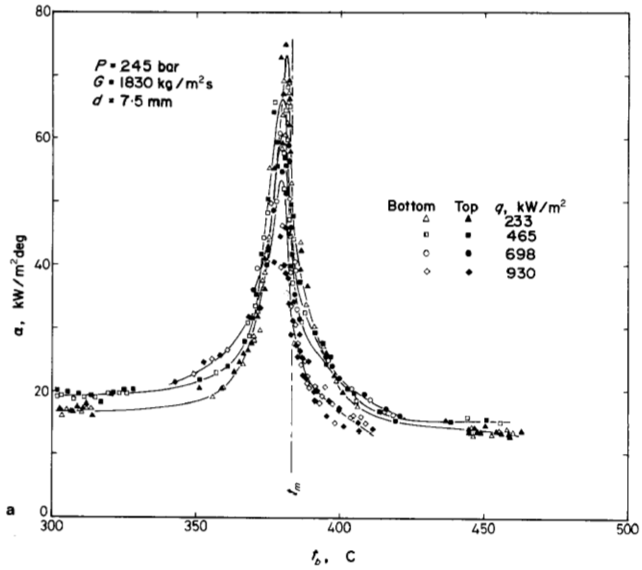

Figure 3: HTC against the bulk temperature in a horizontal flow [16].

three different directions (horizontal, vertical upward and downward) at low heat fluxes (q"<698 kW/m^2). Yamagata et al. [16] also found, in case of vertical upward flow of water, that the HTC in the pseudocritical region becomes higher when the pressure approaches the critical pressure, see Figure 4. Dang [17] found in his research an increase of HTC when the mass flux is increasing. The explanation he gives is that when the mass flux increase there is an increase in turbulent diffusion. By this turbulent diffusion more heat can be transferred from the wall to the fluid.

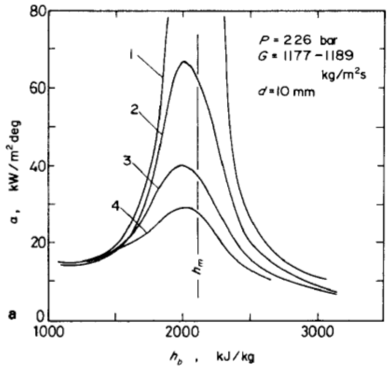

(a)

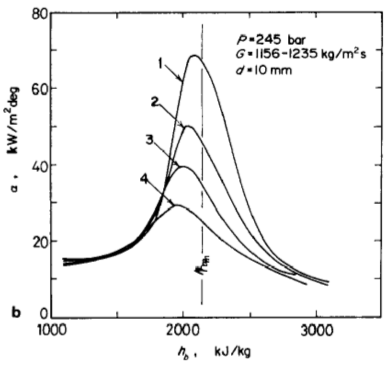

(b)

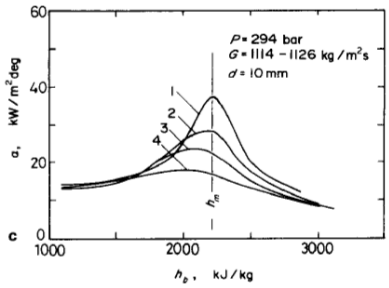

(c)

Figure 4: HTC against bulk enthalpy for vertically upward flow; (a) P=226 bar, (b) P=245 bar and (c) P=294 bar. Where the different lines are HTC results of different heat fluxes: 1)q''=233 kW/m^2; 2. q''=465 kW/m^2; 3. q''=698 kW/m^2; 4. q''=930 kW/m^2 [16]

.

2.1.2 Heat transfer enhancement in SCW

Ackermann (1970) [4; 18] investigated heat transfer to SCW with smooth vertical tubes and tubes with internal ribs. His experiments show that in ribbed tubes the pseudo-film boiling (i.e. low-density fluid prevents high-density fluid from ″rewetting″ a heated surface, this occurs at subcritical pressures) was suppressed. Pseudo-film boiling is due to the large differences in the fluid density, between the wall and the bulk, below the pseudocritical point. In Figure 5(a) the temperature against the bulk fluid enthalpy is shown. In this figure the bulk fluid temperature and inside wall temperatures are presented. The inside wall temperature for the ribbed tubes are presented for two different heat fluxes. The HTCs for these inside wall temperatures are shown in Figure 5(b). The axial temperature profiles in the ribbed tubes show a more continues line and therefore a more continues HTC line against high HTC peaks of the smooth tube, see Figure 5(b). The temperature of the ribbed tube is also lower than the smooth tube due to a higher HTC in the ribbed tube.

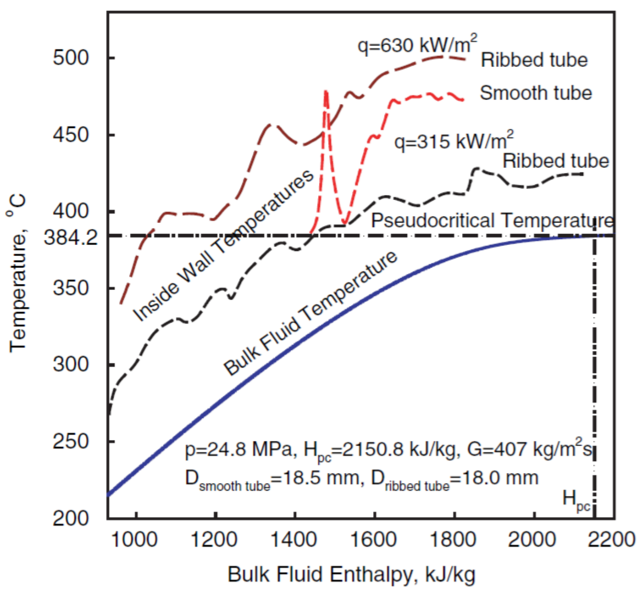

(a)

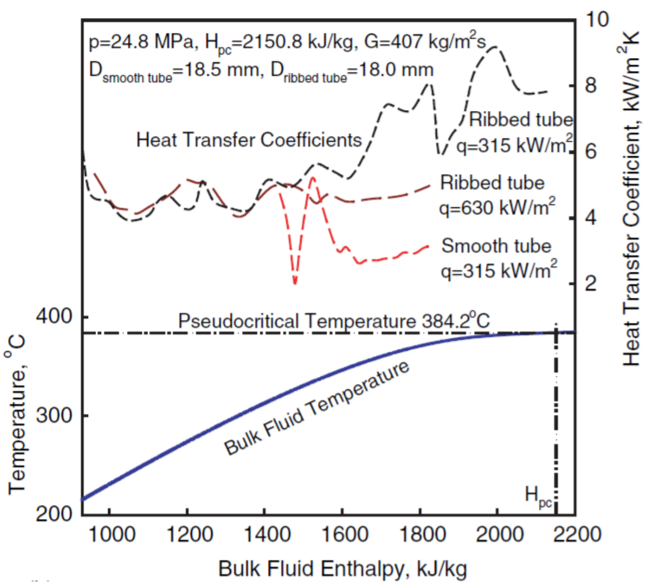

(b)

Figure 5: (a) Temperature against bulk enthalpy and (b) HTC against bulk enthalpy along vertical smooth and ribbed tubes cooled with SCW [4]

Lee and Haller [4; 19] found also this temperature and HTCs behaviour with twisted tubes. The explanation they give, is that the twisted tube cause the flow to spin and therefore centrifugal forces are present. These forces causes a lower temperature and denser fluid to move to the heated wall.

2.2 Critical point of different substances

Pioro and Duffey have listed critical parameters of different fluids, shown in Table 1 [4].

The change in of properties of supercritical solvents are similar as the change in properties of water. This phenomena is used to describe the change in properties of supercritical solvent [4]. The properties of Helium and refrigerant R-134 as function of temperature are shown in Appendix B in the book of Pioro and Duffey and follows the trend of the properties of water. A lot of research is done in SCW but also in supercritical CO_2 [4] and therefore supercritical carbon dioxide will be shortly described and will be compared with SCW.

Table 1: Critical parameters of different fluids [4].

Fluid	p_{cr} MPa	t_{cr} °C	ρ_{cr} kg/m³	$\frac{p_{cr} V_{m\,cr}}{R\,T_{cr}}$
Air	3.8	−140.5	333.3	–
Ammonia (NH_3)	11.333	132.25	225.0	0.243
Argon (Ar)	4.863	−122.46	535.6	0.292
Benzene (C_6H_6)	4.89	288.9	309.0	0.266
iso-Butane (2-Methyl-propane, C_4H_{10})	3.64	134.7	224.4	0.283
Carbon dioxide (CO_2)	7.3773	30.978	467.6	0.274
Di-iso-propyl-cyclo-hexane	1.96	376.9	–	–
Ethanol (C_2H_6O)	6.15	240.8	276.0	0.240
Freon-12 (Di-chloro-di-fluoro-methane, CCl_2F_2)	4.1361	111.97	565.0	0.280
Freon-13B1 (Bromo-tri-fluoro-methane, $CBrF_3$)	3.95	67.0	770.0	–
Freon-22 (Chloro-di-fluoro-methane, $CHClF_2$)	4.99	96.145	523.84	0.264
Freon-114a (1,1-Di-chloro-tetra-fluoro-ethane, $C_2Cl_2F_4$)	3.257	145.68	579.97	–
Freon-134a (1,1,1,2-tetra-fluoro-ethane, CH_2FCF_3)	4.0593	101.06	511.9	–
Helium (He)	0.22746	−267.95	69.641	0.307
n-Heptane (C_7H_{16})	2.736	266.98	232.0	0.260
n-Hexane (C_6H_{14})	3.034	234.67	233.18	0.264
Hydrogen (H_2)	1.315	−239.96	30.118	0.309
Kerosene RT	2.5	392.9	–	–
Methanol (CH_4O)	8.1035	239.45	275.56	0.224
Nitrogen (N_2)	3.3958	−146.96	313.3	0.291
Nitrogen tetroxide (N_2O_4)	10.1	157.9	–	–
n-Octane (C_8H_{18})	2.497	296.17	234.9	0.258
Oxygen (O_2)	5.043	−118.57	436.14	0.308
iso-Pentane	3.396	187.2	236.0	0.268
Poly-methyl-phenyl-siloxane	0.75	502	–	–
RT (jet propulsion fuel)	2.19	395	–	–
Sulphur hexafluoride (SF_6)	3.7546	45.583	743.81	0.277
T-6 (jet propulsion fuel)	2.24	445	–	–
Toluene (C_7H_8)	4.1263	318.6	291.99	0.267
Water (H_2O)	22.064	373.95	322.39	0.243

2.3 Supercritical carbon dioxide

Carbon dioxide is a promising coolant because it is environmentally friendly, safe and has attractive properties on the thermodynamics, such as low viscosity and high heat capacity [17]. For example: as shown in Table 1 carbon dioxide (CO_2) has a lower critical temperature and pressure than water. Looking at the properties of CO_2, as in Figure 6, a good comparison with water can be made. This figure shows different properties of CO_2 which have similar trends and influences of pressure as SCW. The changes of these properties with an increasing pressure become also less pronounced (similar to SCW). The specific heat c_p of CO_2 shows a drastic variation when the temperature become close to the pseudocritical temperature [4; 17].

Fewster and Jackson [18] did CO_2 experiments in the turbulent flow regime (G=300-3300 kg/m^{2}s),see Figure 7. This figure gives the bulk fluid temperature, external wall temperature and the HTC coefficient. Here there are three modes for heat transfer in vertical tubes with upward flow at a pressure of 7.58 MPa, mass flux of 289 kg/m^{2}s and a heat flux of 50-460 kW/m^2:

1. Normal heat transfer
2. Improved heat transfer (i.e. higher than expected HTC values); this takes place in an area where the external wall temperature makes a drop and the bulk fluid temperature is below the critical temperature.
3. Deteriorated heat transfer (i.e. lower than expected HTC values); this may appear at high heat fluxes and lower mass fluxes, and where the external wall temperature increases rapidly. This is also when the bulk fluid temperature is below the critical temperature.

Pioro and Duffey [4] concluded that the heat transfer at supercritical conditions of carbon dioxide is affected with flow directions (upward, downward and horizontal). Experiments in horizontal orientated tube (D=22.1 mm, L=2.4 m) at a flow of 0.035-0.15 kg/s, shows a non-uniform temperature profile in the cross-section of the tube. The buoyancy effect plays a role in the different HTC values in the cross-section. The heat transfer at the bottom of the tube is enhance by the buoyancy effect and at the top it is reduced, because the hotter fluid is in the top of the tube. Yamagata et al. [16] found this phenomenon also for SCW at low heat fluxes.

Pioro and Duffey [4] conducted experiments at a pressure of 7.58 MPa, turbulent flow (G=636 kg/m^{2}s) and different constant heat fluxes (q"=48-64 kW/m^2). They calculated a HTC is between 1000-4000 W/m^{2}K, see Figure 8. In this figure the bulk fluid temperature, external wall temperature and the HTC coefficient are given. Here it is shown that an increase in the heat flux results in a decreasing HTC. Also it is shown that the HTC of CO_2 is nearly constant along

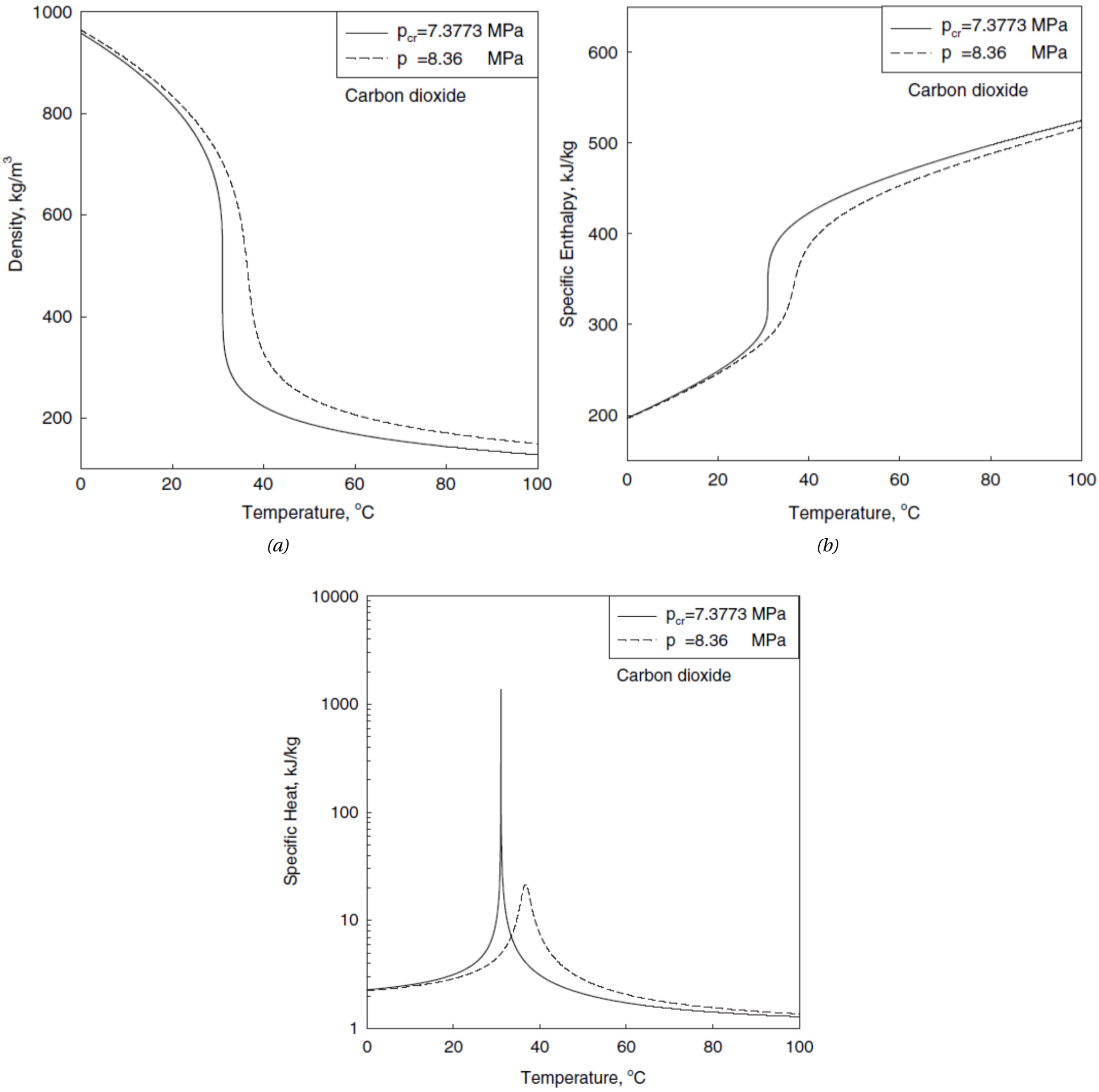

Figure 6: Different properties of carbon dioxide at 7.3773 and 8.36 MPa; (a) Density, (b) Enthalpy and (c) Specific isobaric heat capacity. [4]

the heated length and no maximum of HTC is shown. Pioro and Duffey describe also a deteriorated heat transfer at high heat fluxes and in any place along the heated length. Deteriorated heat transfer corresponds to a lower HTC and a higher external wall temperature.

2.4 Prediction methods for heat transfer

Many correlations for HTC are proposed for SCW, but these are devoted to turbulent supercritical water flows (G>500 kg/m^{2}s). Pioro and Duffey [4] studied many correlations which show quite different results within the same operating range. In 1942, McAdams proposed to use the Dittus and Boelter equation, equation 1, for forced convective heat transfer in turbulent flow and at subcritical pressures and later also at supercritical pressures [4; 3].

$$Nu_b = 0.0243 Re_b^{0.8} Pr_b^{0.4} \tag{1}$$

This correlation is in good agreement with the measured data for supercritical water till 31 MPa and low heat fluxes but

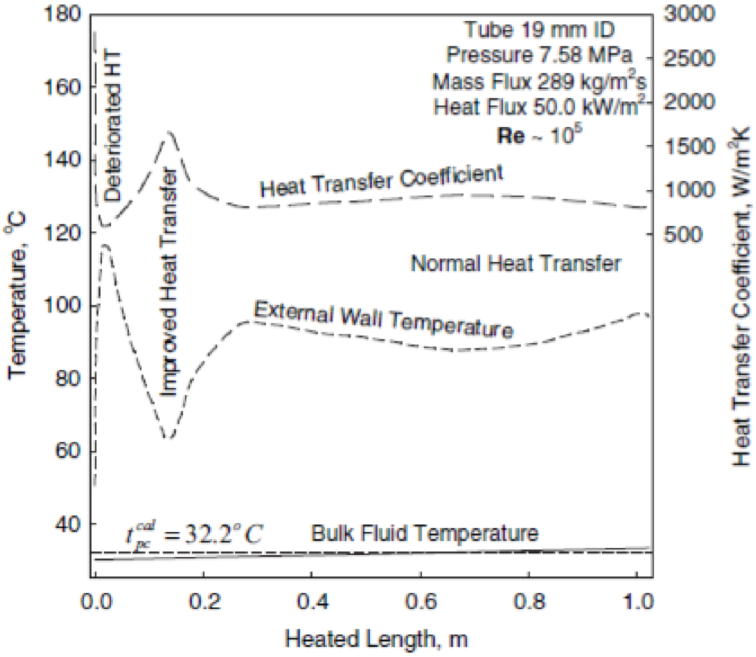

Figure 7: Variations in fluid and wall temperatures and in HTC along heated length [4]: CO_2, circular tube, and upward flow.

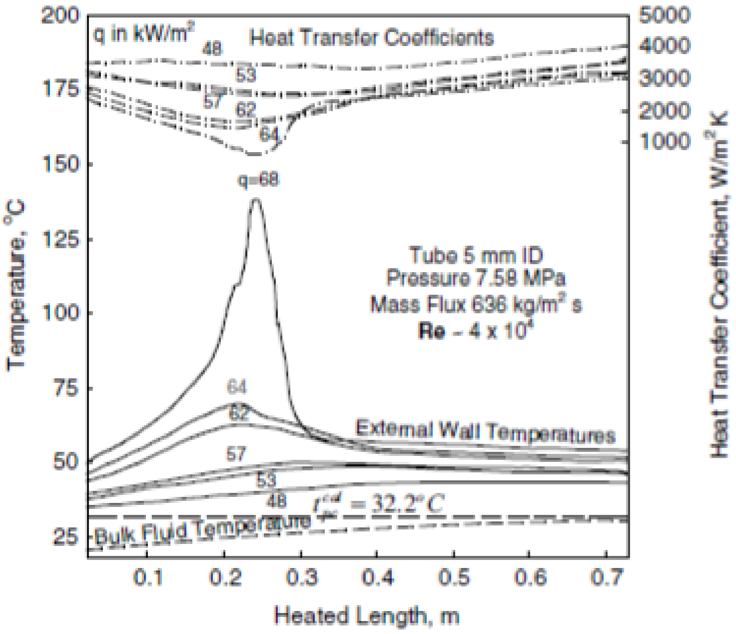

Figure 8: Variations in wall temperatures and in HTC along heated length at various heat fluxes [4]: CO_2, circular tube, and upward flow.

gives unrealistic results near the critical and pseudocritical point [4; 3].

Bishop et al. [20] conducted experiments in upward flow in smooth tubes with the following operating parameters: pressure of 22.8-27.6 MPa, bulk-fluid temperature of 282°C-527°C, mass flux of 651-3662 kg/m^{2}s and heat flux of 0.31-3.46 MW/m^2. They recommend the following correlation, with a fit of ±15%:

$$Nu_x = 0.0069 Re_x^{0.9} \bar{Pr}_x^{0.66} \left(\frac{\rho_w}{\rho_b}\right)^{0.43} \left(1 + 2.4\frac{D}{x}\right) \tag{2}$$

Where x is the axial location along the heated length. The last term corresponds to the entrance effect. Pioro and Duffey [4] described that Swenson et al. derived to almost the same equation as Bishop et al. without the entrance effect.

$$Nu_w = 0.00459 Re_x^{0.923} \bar{Pr}_x^{0.613} \left(\frac{\rho_w}{\rho_b}\right)_x^{0.231} \tag{3}$$

Equation 3 is obtained within the following operating parameters: P=22.8-27.6 MPa, T_w = 93°C-649°C, T_b = 75°C-576°C and G=542-2150 kg/m^2s, and this is within a fit of ±15%. Yamagata et al. [16] found that Equation 3 generally under predicts the experimental HTC.

Morky et al. [3] tested experiment data to the following form for Bishop et al. correlation, without taking the entrance effect into account:

$$Nu_x = 0.0069 Re_x^{0.9} \bar{Pr}_x^{0.66} \left(\frac{\rho_w}{\rho_b}\right)_x^{0.43} \tag{4}$$

The Dittus-Boelter correlation in the form which is in the most widely used interpretation:

$$Nu_b = 0.023 Re_b^{0.8} Pr_b^{0.4} \tag{5}$$

Morky et al. have shown that the correlation of Bishop et al. (equation 4) is in good agreement with the experimental HTCs outside the pseudocritical region. This correlation over predicts with 25% the HTC values within the pseudocritical region. The Dittus-Boelter correlation also predicts the HTC values outside the pseudocritical region good but deviates significantly from the experimental data within the pseudocritical region. This is also found by Pioro and Duffey [4].

The correlations (2)-(5) are based on force convection in the turbulent flow regime. Our research is focussed on low fluxes (G<20 kg/m^2s)in the laminar regime. In laminar flow, heat transport can be either by forced convection or by free (natural) convection, or by combination of the two. In previous research [5] the following correlations on forced and free convection are found in the literature. These correlations are for laminar flow "normal" (atmospheric pressure and subcritical temperatures) conditions.

For laminar forced convection:

$$Nu = 1.86 \left(RePr\frac{d_i}{L}\right)^{0.33} \left(\frac{\mu_b}{\mu_w}\right)^{0.14} = \frac{h_i d_i}{k} \tag{6}$$

And for free convection in vertical systems:

$$Nu_s = f\left(Gr_s^* Pr\right) = \frac{h_i R}{k} \tag{7}$$

Where:

$$Gr_s^* = \frac{g\beta\left(T_{iw} - T_{in}\right) R^3 \rho^2}{\mu^2} \frac{R}{L} \tag{8}$$

$$Pr = \frac{C_p \mu}{k} \tag{9}$$

The Nusselt correlation for a heated tube with a low Grashof numbers ($Gr^*_s < 1$) is given by [5]:

$$Nu_s = 0.0625\left(Gr_s^* Pr\right) \tag{10}$$

And for high Grashof numbers the Nusselt correlation is given by [5]:

$$Nu_s = 0.52\left(Gr_s^* Pr\right)^{1/4} \tag{11}$$

The Nusselt correlation for laminar flow under sub- to supercritical conditions is obtained from Comsol simulations of a vertical heated tube geometry and is describes as equation 12 [21]. This correlation is valid for the conditions which are shown in Table 2.

$$Nu = 0.89 Gr^{0.3} Re^{-0.2} \left(\frac{c_{p_{iw}}}{c_{p_{mc}}}\right)^{0.2} = HTC \frac{d_i}{k_{mc}} \tag{12}$$

Where:

$$Gr = \frac{g\beta_{mc}\left(T_{iw} - T_{mc}\right) d_i^3 \rho_{mc}^2}{\mu_{mc}^2} \tag{13}$$

$$Re = \frac{Gd_i}{\mu_{mc}} \tag{14}$$

Table 2: Parameters for the Nusselt correlation.

Parameter	Value
G (kg/m^{2}s)	7, 20
P (bar)	300
T_{in}(°C)	327
T_{out}(°C)	484
d_i (cm)	1
Re	1000-6500
Gr	$2 * 10^{-7} - 2 * 10^{-8}$
Pr	1.0 - 3.6

3 Experimental section

In this chapter the experimental part of this research will be discussed. In the first part the setup will be described and in the second part the correlations and calculation method to obtain the heat transfer coefficient (HTC) are given.

3.1 Setup design

The experimental setup to study heat transfer coefficient for SCW flow at low mass fluxes (G<20 kg/m^2 s) is a heated vertical tube. In this study demi-water is used to prevent any corrosion and solids deposition in the setup and to make fair comparison with the Comsol simulation. A schematic illustration of the experimental setup is shown in Figure 9.

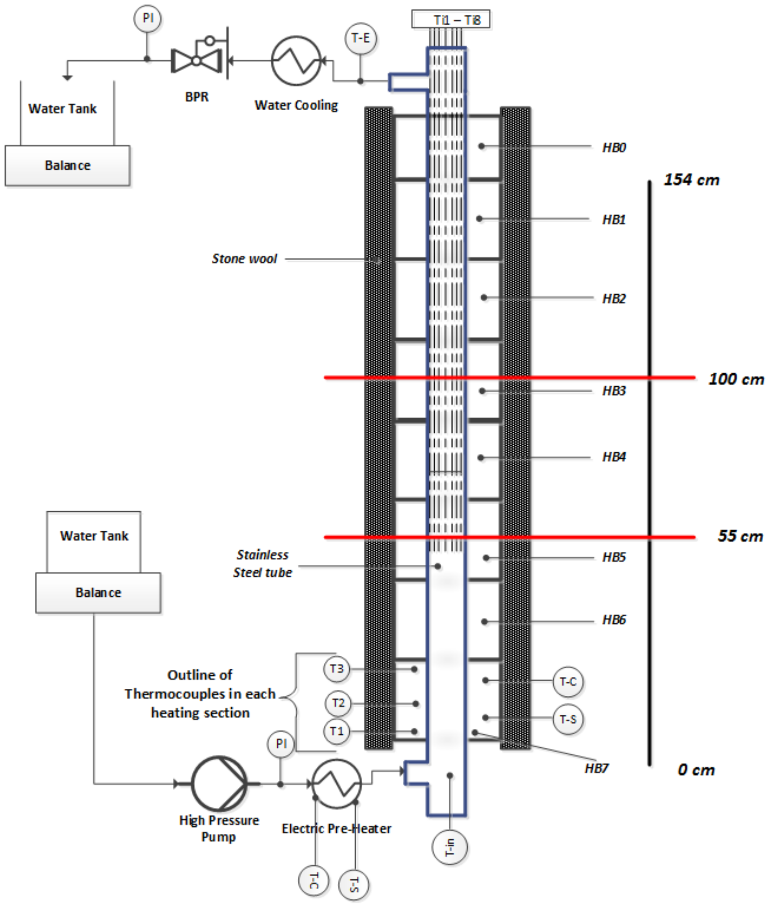

Figure 9: Schematic illustration of the experimental setup with the different specifications.

Demi-water flows from a pressurized vessel (up to 7 bar) via a high pressure pump from LEWA (0- 12 kg/h and maximum pressure of 380 bar), to an electric preheater. The purpose of the preheater is to raise the temperature of water to the desired inlet temperature for the heat exchanger. This preheater has a temperature control (T-C) to set the temperature to the desired inlet temperature, and a temperature safety (T-S) which is used to shut down the pre-heater if the temperature goes above the set value.

The heat exchanger is a stainless steel tube and has the following configuration: outer diameter (OD) of 33.40 mm, inner diameter (ID) of 20.70 mm, wall thickness (t) of 6.35 mm and a length (l) of 1.54 m. The tube is surrounded with 14 aluminium heating blocks (height = 22 cm each) and each one covers half of the tube, so there are 7 heating blocks at each side of the tube. At one side the heating blocks have also T-C and T-S controllers. The heating blocks are insulated from the surroundings with stone wool. At the top of the tube is an additional, smaller (height = 11 cm) heating block installed to prevent back flow at the top of the tube which might arise from cooling and condensing of the SCW before exiting the tube.

To control the high pressure in the tube, a Back Pressure Regulator (BPR) is installed, which can operate up to 400 bar.

This BPR is manually air-controlled from outside the high pressure box. In front of the BPR is a watercooler installed because the BPR is not designed for temperatures higher than 80°C. Pressure indicators are installed at the inlet and outlet of the tube to calculate the pressure drop over the tube.

For the radial temperature profile inside the tube a metal rod is placed with 7 Type K thermocouples ($T_{i,1}$ to $T_{i,7}$) for measurements at a height of 55 cm from the tube inlet and 8 Type K thermocouples ($T_{i,1}$ to $T_{i,8}$) for the height of 100 cm. This is shown in Appendix I. On the outside of the tube 18 thermocouples are placed for the axial temperature profile (T1,T2,T3,..., see Figure 9 at the bottom of the figure). At four axial positions, 11, 33, 55 and 100 cm, thermocouples are placed in the tube wall to measure the temperature gradient in the wall, as shown in Figure 10. Finally, one thermocouple is placed at the inlet for the inlet temperature and one after the water cooler before the BPR. All the data from the thermocouples, except the one for the BPR, are recorded with the data acquisition software (picolog) from Picotech that is connected to a computer.

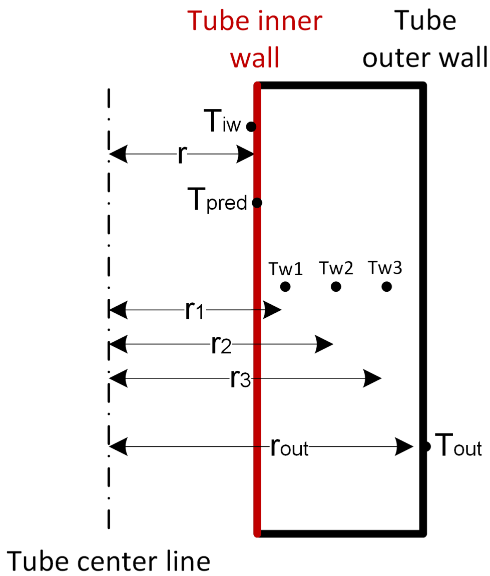

Figure 10: Labelling of the thermocouples positions in radial direction. For the position of: 55 cm r=10.70 mm, r_1=11.70 mm, r_2=13.70 mm, r_3=15.70 mm and r_{out}=17.05 mm from the tube center line. For the position of 100 cm: r_{it}=10.70 mm, r_1=11.45 mm, r_2=13.64 mm, r_3=14.75 mm and r_{out}=17.05 mm from the tube center line.

During experiments the radial temperature profile can only be measured at one axial position. The radial temperature profile is measured at two different heights: 55 cm and 100 cm. These heights are measured from the bottom of the tube to the top, see the red lines in Figure 9. The heating blocks are numbered from 7 to 0 from the bottom to the top. The middle of heating block 5 is at 55 cm and the middle of heating block 3 is at a height of 100 cm.

3.2 Operating procedure

Before starting an experiment it is necessary to ensure that there is enough water in the water tank and to adjust the metal rod, which is holding the thermocouples for radial temperature measurements inside the tube, to the required axial position. After adjusting the axial position of the thermocouple holder, the pump is switched on to check if there are no leakages. Before switching on the heating blocks the cooling water must be switched on. Also the webcams and thermocouple measurements have to be checked.

The pressure is increased with steps of 25-50 bar to the desired operating pressure. If the right pressure is reached, the heating blocks are switch on one by one and set to their desired temperature. If the temperature readings are constant (± 2°C for 5 min) the temperature measurement can start.

During the measurements the pressure, temperatures and webcam have to be monitored, to see if there are no leakages, pump failures or other dangerous situations.

3.3 Calculation procedure

In previous research [5], on laminar flow, an indirect method is used to calculate the heat transfer coefficient. This indirect method is based on enthalpy changes in the water flow, see Figure 11. In this report a more direct method is used, namely based on the calculation of the heat flux through the tube wall from the experimental wall temperatures.

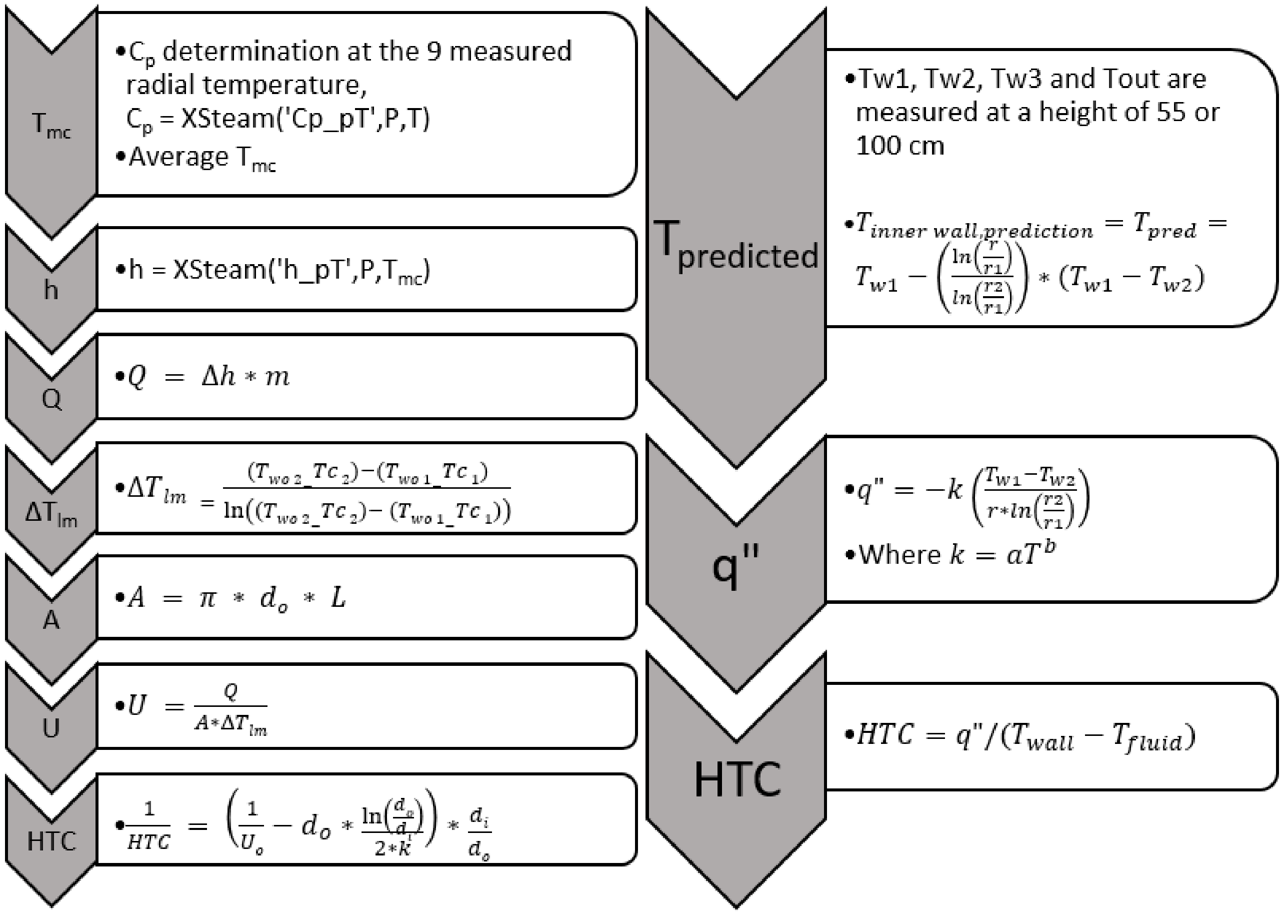

Figure 11: Calculation procedure of [a]: Raghda et al.[5] and [b]: this research.

The heat transfer coefficient (HTC) is a quantitative number which describes the heat transfer between a surface (wall)and a fluid medium [22]. In this research this medium is inside of the tube and is sub- and supercritical water. HTC is defined as:

$$HTC = \frac{q"}{T_{wall} - T_{fluid}} \tag{15}$$

Where HTC is the heat transfer coefficient in W/(m^{2}K), q$''$ is the heat flux in W/m^2, T_{wall} is the wall temperature inside the tube and this wall temperature can either be measured with the thermocouples attached to the probe or predicted with extrapolation of T_{w1} and T_{w2} or T_{out} . T_{fluid} is the liquid temperature and is the experimental measured center bulk temperature or the mixing cup temperature. The mixing cup temperature is the average of the measured temperatures of the fluid over the cross section [23]. The temperature is depending on radial direction and axial direction [23]. The mixing cup temperature (T_{mc}), when a negligible axial conduction is assumed, is defined as:

$$T_{mc} = \frac{\int_A \rho u C_p T \, \mathrm{d}A}{\int_A \rho u C_p \, \mathrm{d}A} \tag{16}$$

The heat flux, q″, is defined as [24]:

$$q'' = -k\nabla T \tag{17}$$

$$q'' = -k\left(\frac{T_{w1} - T_{w2}}{r * \ln\left(\frac{r_2}{r_1}\right)}\right) \tag{18}$$

The temperature gradient is based on experimental temperature measurements inside the cylindrical tube wall. The tip positions of the thermocouples are r_1 and r_2 from the centre of the tube, see Figure 10.

Where k is the thermal conductivity, W/mK, which is a function of the average temperature of the wall according to, equation 19.

$$k = aT^b \tag{19}$$

T is the average wall temperature in Kelvin, and the constants a=1.22 and b=0.432 [25].

For the HTC the inner wall temperature must be determined, because the heat transfer is from the inner wall to the fluid. It is difficult to measure the exact temperature at the inside of the wall therefore different methods are used to determine the temperature of the wall. The first method measures the temperature with a thermocouple from the fluid side. One of the drawbacks of this method is that the sensitivity of the tip of the thermocouple is 0.5 mm, so not only the temperature of the wall is measured but also a part of the fluid. Also the line-up of the thermocouple against the wall is unknown. The second drawback is the probe, the place where the thermocouples are place at the metal rod, that can influence the flow profile and therefore the temperature profile. The last drawback is that there is a local turbulence at some locations, such as location near the wall. This is causes by natural convection i.e. buoyancy effect. These local turbulences are at the experimental conditions and therefore the flow pattern is unknown. Therefore it also unknown if fluid from lower or higher position has influence on the temperature at a certain/experimental height. Because the first method has some drawbacks a second method is applied to predict the inner wall temperature at the interface. This second method calculates the inner wall temperature assuming Fourier's law, with temperature measurements inside the wall, see Figure 10. This method is used to predict the interface wall temperature.

The heat transferred from position r_1 to r must, by the first law of thermodynamics, be equal to r_2 to r_1. The temperatures inside the wall are measured and using Equation 20 a prediction can be made for the temperature at the inner wall of the tube:

$$T_{inner wall,predicted} = T_{w1} - \left(\frac{\ln\left(\frac{r}{r_1}\right)}{\ln\left(\frac{r_2}{r_1}\right)} * (T_{w1} - T_{w2})\right) \tag{20}$$

3.4 Nusselt correlation for sub- and supercritical water flow

In the previous chapter is prediction methods for heat transfer in the turbulent region were discussed. In this research the focus is on heat transfer at low mass fluxes, in the laminar flow regime. In previous research [21] it is shown that natural convection becomes more dominant and important in laminar flow. A new Nusselt correlation was obtained from Comsol simulations, equation (12) to (14). With this correlation the HTCs can be simulated and compared with experimental HTCs.

Equation 12 is based on the calculated properties of water at the mixing cup temperature, equation 16, and the operating pressure. $C_{p_{iw}}$ is calculated for the predicted inner wall temperature, T_{iw} prediction is based on the measured radial temperature profile in the tube wall. The parameters under which this correlation was derived are listed in Table 2. This correlation fits the results obtained from a Comsol model that describes the experimental setup for an inside diameter up to 2 cm at a mass flux of 7 and 20 kg/m^{2}s within ± 15% error. [5]

3.5 Thermocouple error determination

The absolute error in the Type-K thermocouples is experimentally determined. Four thermocouples were placed in a copper heating block for uniform heating. Three thermocouples, which were taken from the setup, have already been subjected to high temperatures during previous experiments. These three thermocouples are from the same batch and the fourth thermocouple is from a new batch without any high treatment. The temperature of the copper heating block was set at 300°C. When steady state was reached, temperature measurements of these thermocouples were recorded for 4 minutes.

In Appendix IV, Figure 38 shows the temperature measurement over time. The fluctuations in temperature over time is due to the temperature control of the heating block. These fluctuations are the same for all four thermocouples, therefore the results were averaged for each thermocouple. The average of the three old thermocouples (from the setup and the same batch) is 303.58°C and the absolute error is ±0.10°C.

A correction factor of 2.30°C is added to the average temperature of the new thermocouple. This correction factor is found experimentally in a steady state surroundings. In this experiment different thermocouples of two batches are placed in water and heated till 90°C and had a temperature difference of 2.30°C. The average temperature of the fourth thermocouple is (after adding the correction factor) 303.36°C. The average temperature of all four thermocouples (old and new together) is 303.52°C. With this average temperature an absolute error of ±0.15°C is obtained.

For the position of the thermocouple, radius r, is measured with a Vernier Calliper and therefore the (possible) error is ±0.05 mm.

4 Results

The experimental research is divided in two parts: temperature measurements (axial, radial in the wall and radial in the fluid using the probe) carried out at a height of 55 cm or at a height of 100 cm. At these axial positions a wide range of experiments are performed with different flow rates, inlet temperatures, outer wall temperatures and pressures. In this research three different flow rates are used: 4.1 kg/h (G=3.2 kg/m^{2}s), 8.0 kg/h (G=6.2 kg/m^{2}s) and 11.3 kg/h (G=8.8 kg/m^{2}s). In this report the flow rates are presented as 4, 8 and 11 kg/h, respectively.

4.1 Experimental results at a height of 55 cm

In each of the experiments, temperatures were measured in axial and radial direction (in the wall and fluid). At 55 cm, the wall thermocouples are located at the middle of the heating block 5, see Figure 9. The setting of heating block 6 (below heating block 5) is 10°C lower than heating block 5 to get a visible radial temperature gradient in the water.

From each of the experiments an axial temperature profile is obtained. These temperatures are the temperatures at the outer wall of the tube in the axial direction, examples are Figure 12 and Figure 19. In this figure a steep temperature gradient is shown in the first 30 cm, due to the good heat transfer of the wall to the fluid in this part. After 55 cm the temperature become more or less constant, which means that the wall and the heating blocks have the same temperature and there is no fast heat transport.

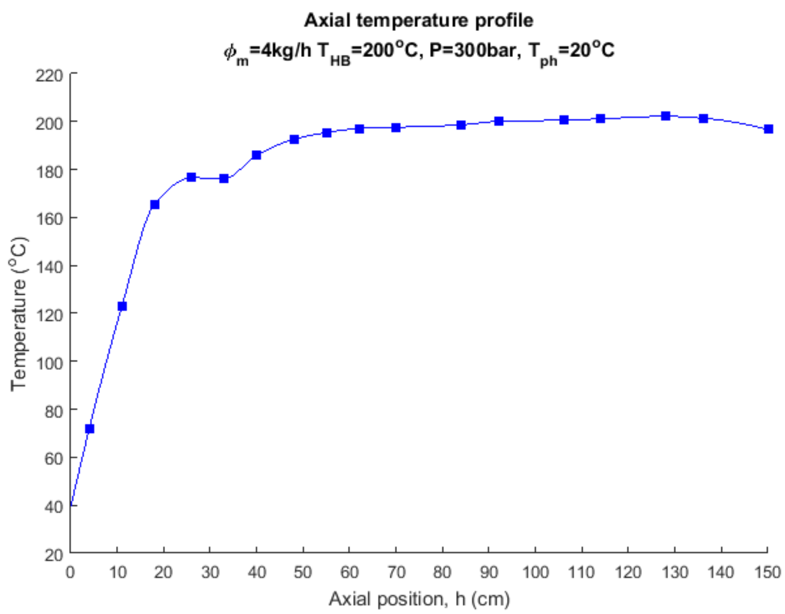

Figure 12: Axial temperature profile with a flow rate of 4 kg/h and pressure of 300 bar.

At the axial position of 55 cm the radial temperature profile in the wall and fluid is obtained, Figure 13. In this figure, the temperatures in the fluid (left side) and the wall (right side) are shown. In the fluid a steep temperature gradient is shown at the wall, this is in line with previous research [6]. In the wall a slightly curved temperature profile is visible and this is in line with the heat transfer in cylindrical coordinates. T_{w3} is not shown in this figure, because the thermocouple was not in the right position to measure the temperature correctly. Two different inner wall temperature predictions are shown in Figure 13. The star represents the predicted value based on the measured values inside the wall (T_{w1} and T_{w2}). The solid black dot is predicted based on the outer wall and the temperature deepest in the wall (T_{w1} and T_{out}). Both predictions are very close, see also Appendix II: Figure 36. This is as expected because all the heat will be transferred from the outer wall to the fluid. It that case it does not matter with which temperatures the heat flux will be calculated. At the height of 55 cm the temperatures inside the wall (T_{w1} and T_{w2}) are chosen for calculating the heat flux and for predicting the inner wall temperature. In Figure 13, the measured temperature at the wall (blue star) is close to the predicted values. The thermocouples in the fluid, which are against the wall (T_{i1} and T_{i2}), are measuring the wall as well the fluid and therefore the measured inner wall temperature is lower than the predicted inner wall temperature. The predicted inner wall temperature is not influence by the fluid and therefore this temperature is more accurate. At the radius of 0 mm the center bulk temperature is measured which will be used in the calculations and plots.

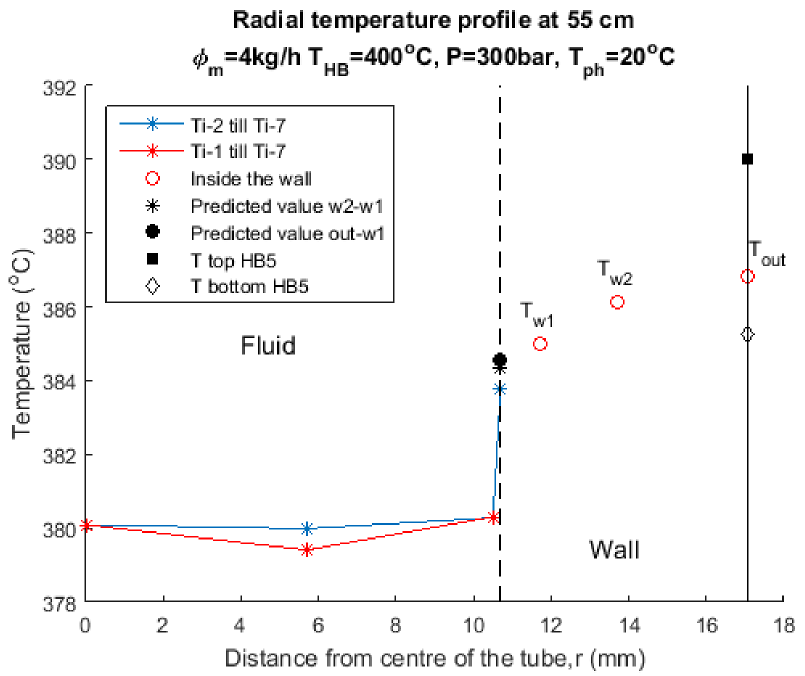

Figure 13: Radial temperature profile at a height of 55 cm, flow rate of 4 kg/h and pressure of 300 bar.

In Figure 14 the $HTC_{measured}$ and the $HTC_{predicted}$ are shown against the center bulk temperature. The blue star solid line is the HTC based on the measured inner wall temperature (with the wall thermocouple in the probe) and the blue circle dashed line is based on the predicted inner wall temperature. The predicted inner wall temperature is based on the inside wall temperature; T_{w1}, T_{w2}, equation 20. The heat flux is in all cases calculated from the temperatures T_{w1} and T_{w2}, equation 18. On the right y-axis the Δ T is shown against the center bulk temperature. Δ T = $T_{inner wall,measured}$ - $T_{center bulk}$ and $T_{inner wall,predicted}$ - $T_{center bulk}$.

The temperature differences, shown in Figure 14, are the driving force for the HTC, see equation 15. At lower bulk temperatures the difference between the Δ T is within 1°C. The deviation between these driving forces lies around the pseudocritical temperature. The driving force for $HTC_{measured}$ is decreasing with an increasing center bulk temperature. The driving force for $HTC_{predicted}$ first increases followed by a dip around the pseudocritical temperature which is due to the good heat transfer around the pseudocritical temperature. This dip in driving forces results in a peak in the HTC.

At subcritical center temperatures the HTC values of the $HTC_{measured}$ and the $HTC_{predicted}$ are close to each other. When the fluid temperature approaches the critical temperature, the HTC based on the measured inner wall temperature increases rapidly and the error in the $HTCs_{measured}$ become larger, due to the smaller temperature difference between the wall and the fluid. The thermocouples of the probe at the wall (T_{i1} and T_{i2}) are more influenced, around the critical temperature, by the fluid temperature than the wall temperature. In Figure 15 the $HTC_{predicted}$ is compared with the correlation (obtained in previous research). Here the $HTCs_{predicted}$, at subcritical temperatures, fits the correlation. For these reasons the predicted wall temperature will be used to calculate the HTC.

In Figure 15 the $HTC_{predicted}$ is compared. Also the correlation with the driving force for the HTC calculation is plotted. These driving forces have a dip around the pseudocritical point, which give the $HTC_{predicted}$ a peak at 387°C, 5 kW/(m^{2}K). This peak lies between the critical temperature and the pseudocritical temperature of water at 300 bar ($T_{pseudocritical}$, 300 bar = 402°C). Yamagata et al. [16] has also reported this peak in the HTC for water between the critical and pseudocritical temperature at 245 bar.

In the subcritical temperature range the HTCs from the correlation and the HTC calculated from the predicted inner wall temperature are in the same order of magnitude. When the temperature approaches the critical temperature more deviation in the HTCs is shown.

The experimental results are always above the correlation but at the subcritical temperatures within the error. Around the critical temperature the correlation shows a strange behaviour this is due to the dip of the driving force. In the correlation, equation 12, the Grashof correlation is represented and the Grashof correlation is a function of the driving forces, equation 21. This causes the dip in the correlation result. The mass flux of the flow rate of 4 kg/h is below the

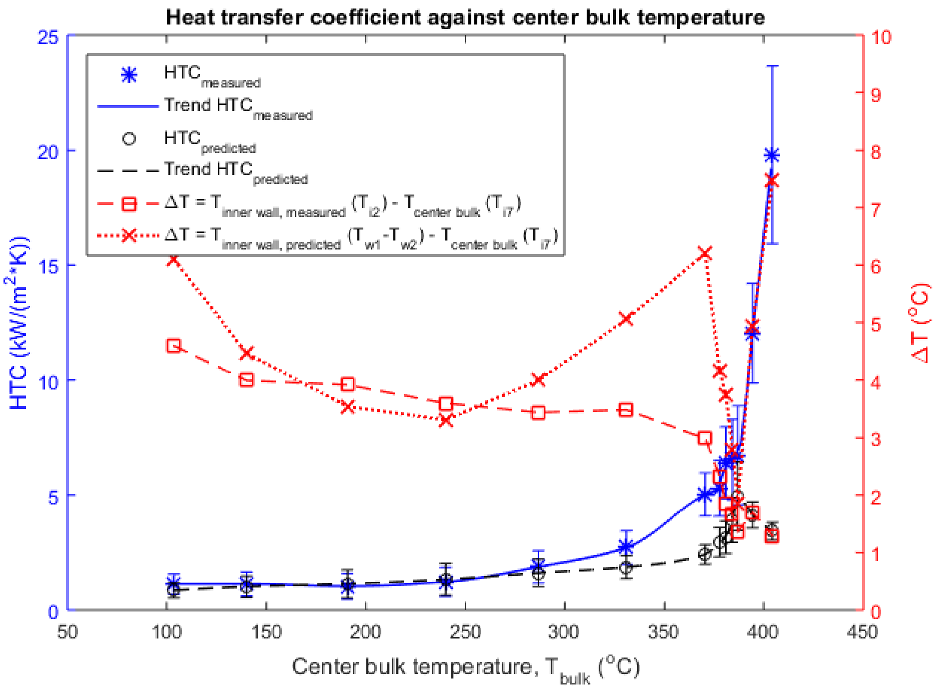

Figure 14: HTC calculations based on i) the measured inner wall temperature line (star blue solid line) and ii) the predicted inner wall temperature (circle black dashed line). The driving forces of i) $HTC_{measured}$ and ii) $HTC_{predicted}$ are shown on the right y-asis. Experimental parameters: H=55cm, P=300 bar, and φ_{water}=4 kg/h.

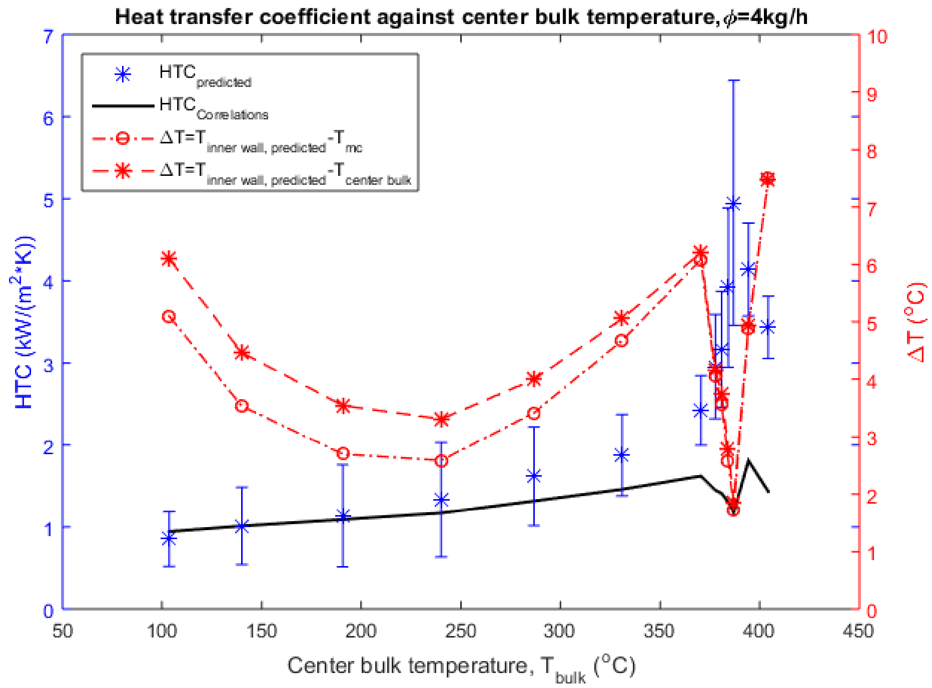

Figure 15: HTC calculations based on i) the predicted inner wall temperature (star blue solid line) and ii) the correlation (solid black line). The driving forces are plotted on the right y-axis. Experimental parameters: H=55cm, P=300 bar and φ_{water}=4 kg/h.

range which is given in Table 2.

$$Gr = \frac{g\beta_{mc}\left(T_{iw} - T_{mc}\right) d_i^3 \rho_{mc}^2}{\mu_{mc}^2} \tag{21}$$

Effect of flow rate

Previous result were obtained with experiments at a flow rate of 4 kg/h. The experimental HTCs and HTCs obtained with the correlation at a flow rate of 8 kg/h are shown in Figure 16. In this figure also the driving forces are shown at the right y-axis. The heat flux is based on T_{w1} and T_{w2} in analogy with the flow rate of 4 kg/h. It is seen that in case of the 8 kg/h no peak in the experimental HTC is obtained, probably due to the operating temperate which does not exceed the pseudocritical temperature. In Figure 16 the experimental results are above the results from the correlation, but the result from the correlation are in the same order of magnitude as the experimental results up to 320°C. At higher temperatures the HTCs start to deviate; the experimental HTC increase and the correlation HTC decrease. This decrease can be explained by the fact that the temperature difference between the bulk and the inner wall prediction become smaller, as shown in Figure 16.

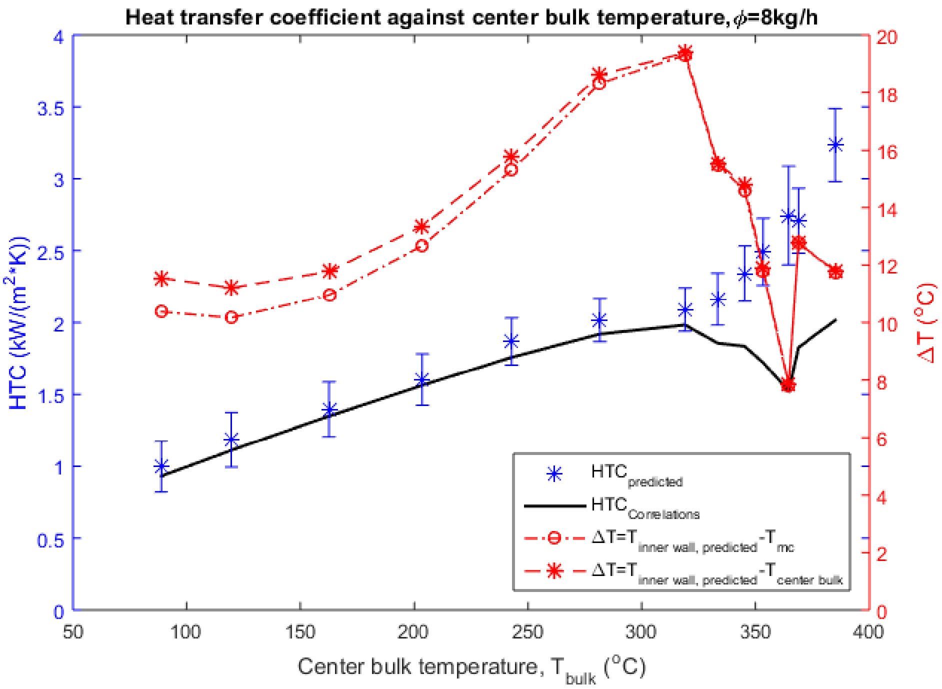

Figure 16: HTC calculations based on i) the predicted inner wall temperature (star blue solid line) and ii) the correlation (solid black line). The driving forces are plotted on the right y-axis. Experimental parameters: H=55cm, P=300 bar and φ_{water}=8 kg/h.

The results of the HTCs and there driving forces at a flow rate of 11 kg/h are shown in Figure 17. Here T_{w1} and T_{w2} are again used to calculate the heat flux. No real maximum in HTC value is obtained, since the operating temperature did not reach the pseudocritical temperature of water. A higher operating temperature is not possible because the heating power below 55 cm is not sufficient. The HTCs shows a decrease between 250°C and 300°C. The experiments of these data points were obtained in two days (two different experimental runs), while the 4 and 8 kg/h are obtained within one experimental run. In the two days the operating pressures were within the fluctuations (± 10 bar) and the start-up procedure was the same. The difference is the starting point of the experimental run. It cannot be said that these results are made in the same conditions; i.e. inlet temperature. Therefore it is important to perform supercritical heat transfer experiments in one sufficiently long experimental run. In general, the experimental HTC is above the HTC of the correlation and is increasing by increasing center bulk temperature.

In Figure 18 the experimental HTCs for all flows, including the HTC of the correlations are shown. This figure shows an increase of the HTC when the mass flow increases, due to more fluid per unit of time passed the tube there is more heat absorbed. This is also found in the HTCs of the correlation. This is also seen by Scalabrin et al. for the heat transfer to carbon dioxide [26]. Dang [17] found an increase of HTC when the mass flux is increasing, due to the increase in turbulent diffusion. The remark on the conclusions of Scalabrin et al. and Dang is that they both have a constant heat flux. In the experiments of this research the heat flux changes ($15.4*10^3$-$81.5*10^3$ W/m^2) with a changing flow rate and therefore changing HTC.

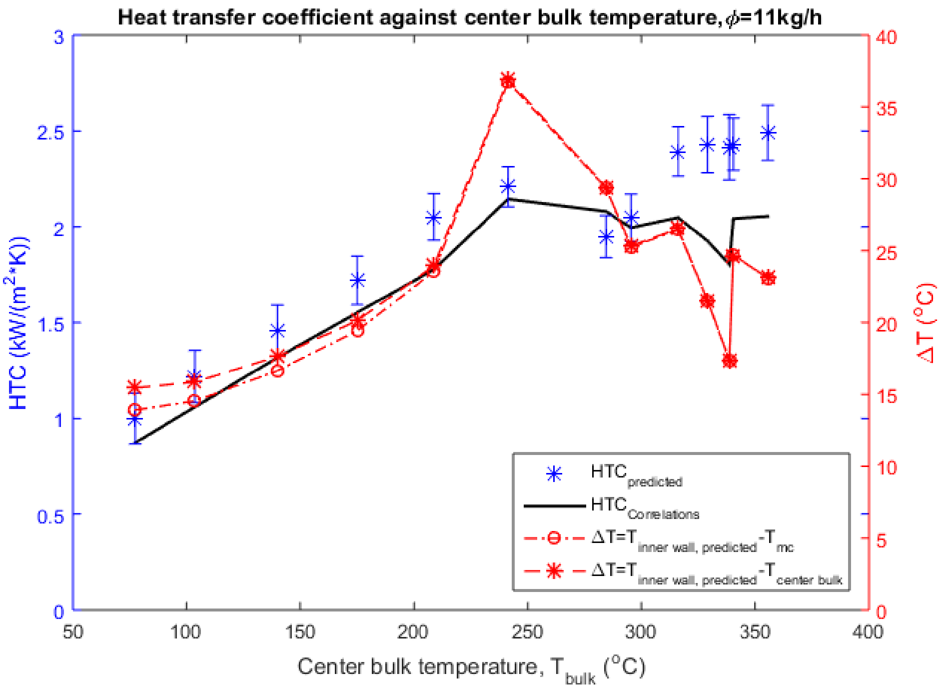

Figure 17: HTC calculations based on i) the predicted inner wall temperature (star blue solid line) and ii) the correlation (solid black line). The driving forces are plotted on the right y-axis. Experimental parameters: H=55cm, P=300 bar and φ_{water}=11 kg/h.

The maximum centre bulk temperature is restricted by the inlet heating power at a flow of 8 and 11 kg/h. This is the most probably reason why no maximum in HTC is obtained. Therefore a new serie of measurements is repeated at a higher position (at 100 cm).

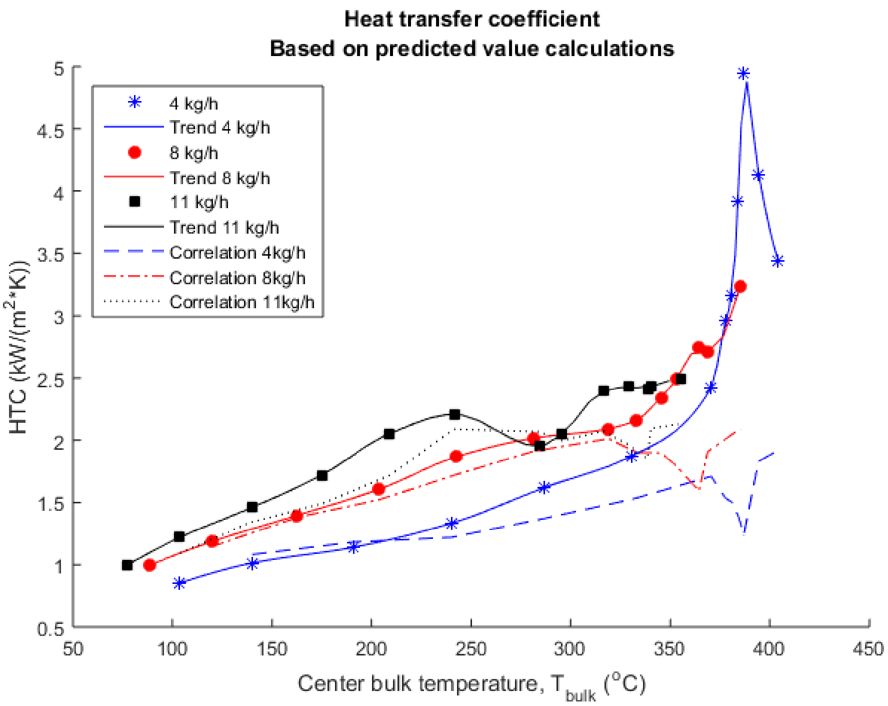

Figure 18: HTC for three different flowrates; 4 kg/h, 8 kg/h and 11 kg/h, P=300bar, H=55cm.

Effect of pressure

Experiments at a pressure of 230 bar were repeated with heating block temperature of 400°C, a preheater temperature range of 20-350°C and flow rates of 4, 8 and 11 kg/h. The HTC results which were obtained where around the (pseudo-)critical temperature. Due to the strong change of the physical properties around the critical point, there is a large fluctuation of the HTCs. The results are shown in Appendix II.

New experiments are done at the height of 100 cm to get a higher temperature range and at a higher pressure (250 bar and 300 bar) to reduce the fluctuation in the results when the temperature become close to the critical temperature.

4.2 Experimental results at a height of 100 cm

At the middle of heating block 3 the thermocouples in the wall are located at 100 cm from the inlet, see Figure **??** for the exact depth. The temperature setting of heating block 4, just below heating block 3, is 40°C lower than heating block 3. The reason for a higher temperature difference is to create a bigger radial temperature gradient in the fluid, especially for the lower pressure of 250 bar. Furthermore all measurements, at a specific flow rate and pressure, are performed in the same experimental run.

For each of the experiments at 100 cm also an axial temperature profile is obtained. These temperatures are the temperatures at the outside of the tube in the axial direction, an example is Figure 19. In this figure a less steep temperature gradient is shown compared the the experiment at 55 cm, due to the temperature settings in the first 60 cm as described before.

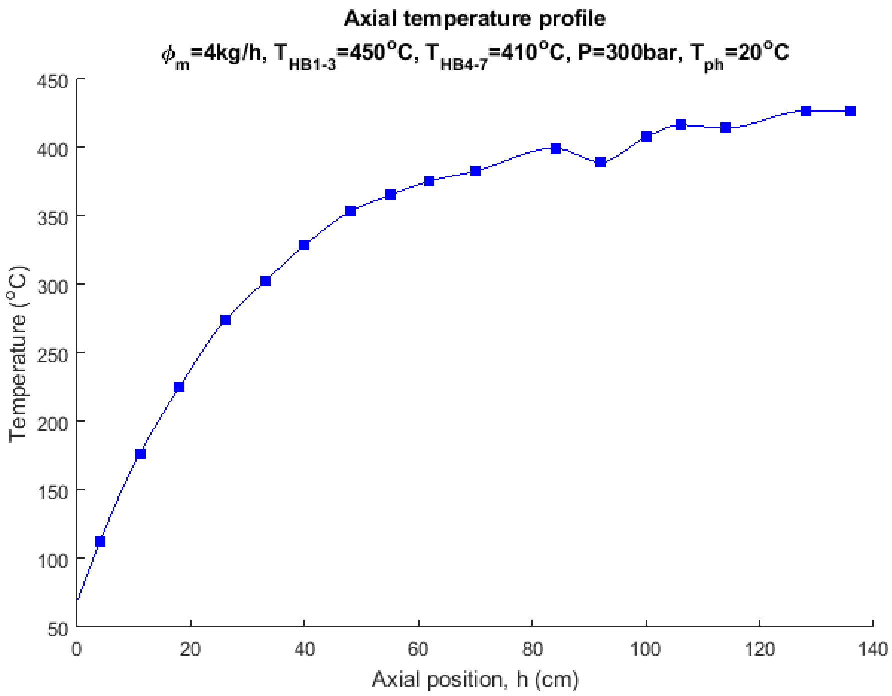

Figure 19: Axial temperature profile at 100 cm with a flow rate of 4 kg/h and pressure of 300 bar. With heating block temperature settings: HB1-3: 450°C, HB4-7: 410°C.

Figure 20 shows two examples of radial temperature profiles obtained in the subcritical region at 100 cm. These figures show a similar temperature profiles in the fluid and the wall, comparable to the measurements at 55 cm. The predicted inner wall temperature based on the inside wall temperature (T_{w1} and T_{w2}) is on top of the predicted inner wall temperature based on temperatures T_{w1} and T_{out}.

Figure 21 shows the radial temperature profile at the sub- to supercritical temperature level. It shows a maximum in inside wall temperature which is higher than the outer wall (the outer wall is heated). This is not as expected and different setup checks were done; temperature readings for existing and new thermocouples and depth control of the thermocouples' holes. These checks showed that there are no mistakes in the thermocouples measurements and the

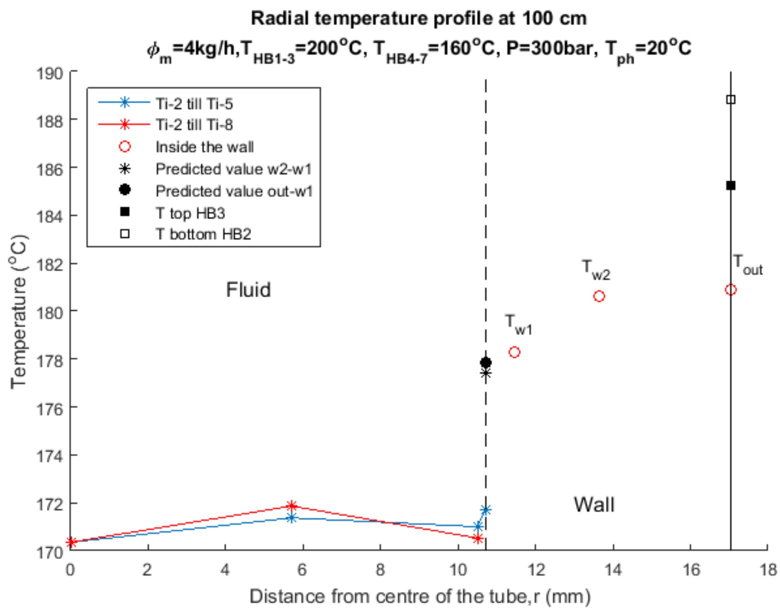

(a)

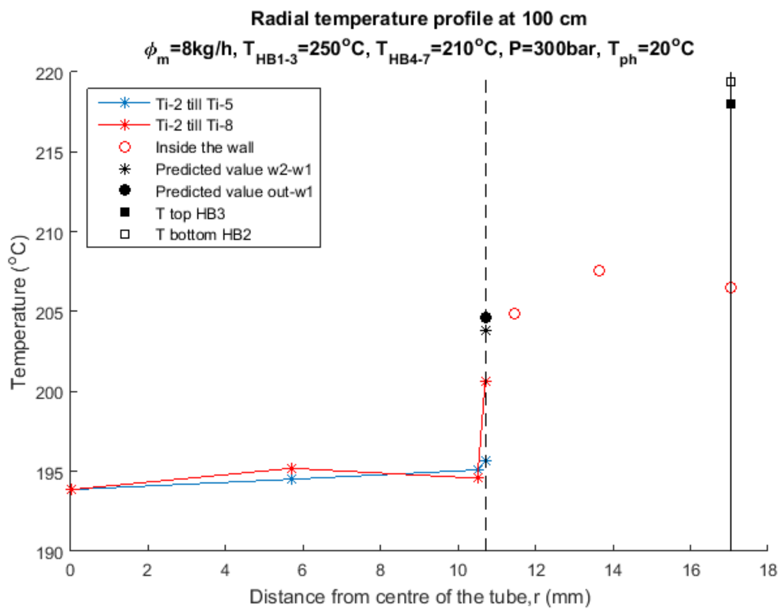

(b)

Figure 20: [a]: Subcritical radial temperature profile at H=100cm, P=300 bar and φ_{water}=4 kg/h. [b]: Subcritical radial temperature profile at H=100cm, P=300 bar and φ_{water}=8 kg/h.

position of the thermocouples. An explanation for this maximum in the wall temperature profile might be an axial heat flow. In Appendix III this explanation is supported by experimental data. Furthermore it is also investigated if some magnetic fields has influence on the temperature readings. This is examined by switching off the heating blocks. Results show there was still a similar temperature profile in the wall as in Figure 21. So no magnetic field are influencing the temperature readings.

Figure 22 shows a schematic overview of a section of the tube with heat transfer in axial and radial direction. On the right side, heat is supplied from the heating block to the tube; $Q''_{r,hot}$. At the left side, water is transported along the inside of the tube where heat is subtracted from the tube; $Q''_{r,cold}$. When the heat supply is larger then the heat withdrawal ($Q''_{r,hot} > Q''_{r,cold}$) energy has to go to another direction, the axial direction. As shown in Figure 19 (especially at 100 cm) the temperature at higher position is larger than a lower position. Therefore heat will be transported in

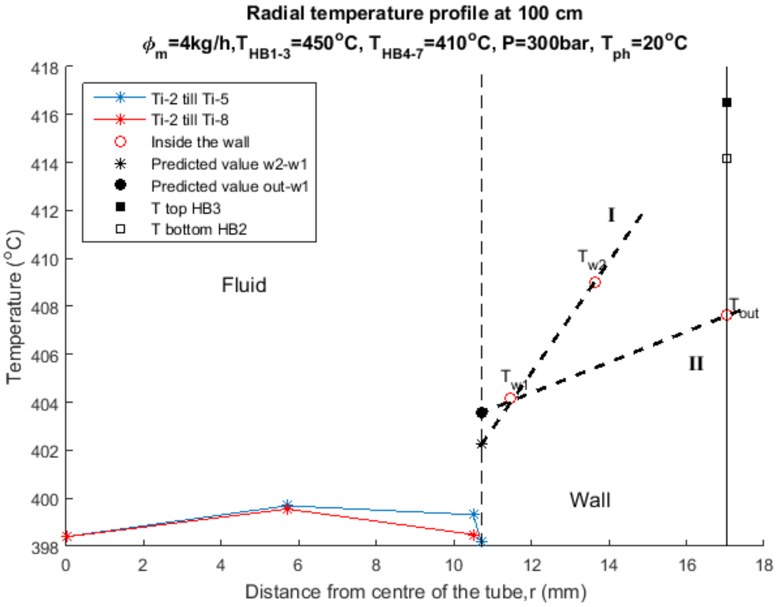

(a)

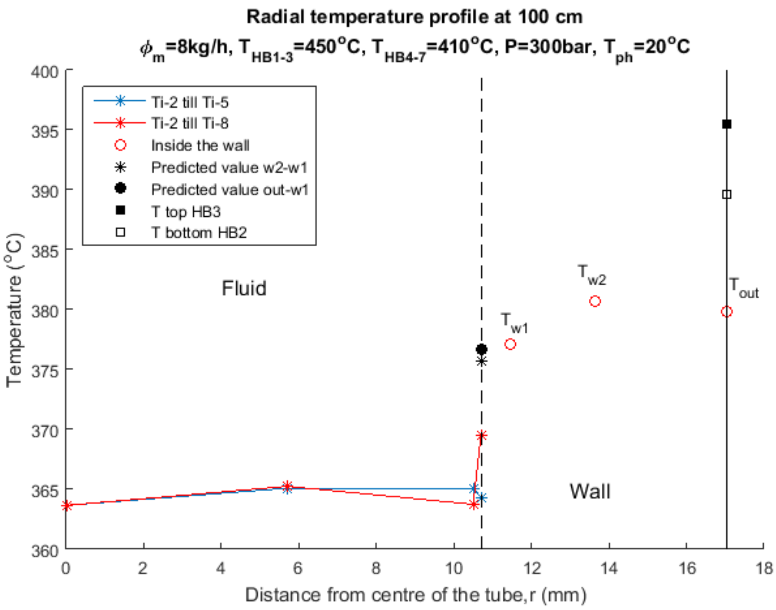

(b)

Figure 21: [a]: Supercritical radial temperature profile at H=100cm, P=300 bar and φ_{water}=4 kg/h. [b]: Supercritical radial temperature profile at H=100cm, P=300 bar and φ_{water}=8 kg/h.

downward vertical direction ($Q''_{z,hot}$ to $Q''_{z,cold}$). In the ideal case heat supply, in radial direction, is the same than the heat withdrawal ($Q''_{r,hot} \leq Q''_{r,cold}$) which results in no axial heat flow if the axial temperature is constant. In the most unfavourable situation the heat supply is much larger than the heat withdrawal ($Q''_{r,hot} \gg Q''_{r,cold}$) and this will results in axial heat transport.

A strong decrease in HTC is shown when the fluid is fully supercritical, see Figure 15 and 18 (for 4 kg/h) at T>380°C. Below the (pseudo-)critical temperature heat transfer from the wall to the water ($Q''_{r,hot} \leq Q''_{r,cold}$, Figure 22) is good. Therefore there is a strong heat transport in radial direction and directly a lower outer wall temperature. This is the case in the first 40 cm of the setup, see Figure 19. At the critical temperature the heat transfer is very good and above the critical temperature the heat transfer will decrease and becomes bad, see Figures 3 and 4. That means that the heat supplied above the critical temperature is not transferred fast enough to the supercritical water. The energy transport

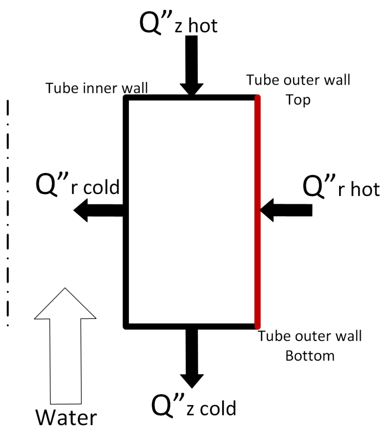

Figure 22: Schematic overview a section of the tube with heat transfer at supercritical water conditions.

in the radial direction is not fast enough and the heat will therefore be transported in vertical direction (Q''_z of Figure 22). The vertical heat transport is now dominant because the radial transport has limitations and the energy takes the way of least resistance.

The hypothesis of vertical heat transfer is also checked by Comsol simulations. A wall temperature profile is found that is comparable in shape to the wall temperature profile shown in Figure 21. This profile is only obtained when also heat is supplied from a lower section, see Figure 23. It is strange that heat is supplied from a lower and colder section of the tube to get the same temperature profile inside the wall. So it is still unknown what really happens inside the wall.

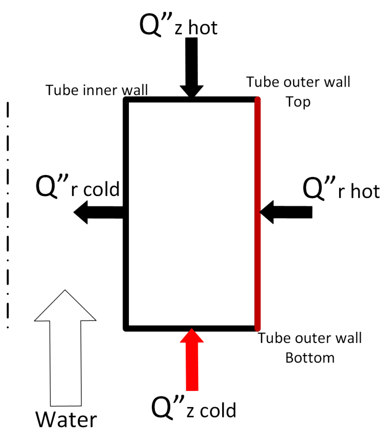

Figure 23: Schematic overview a section of the tube with heat supply from a higher and lower the wall section and heating block (rigth side).

It is unknown how much heat is be transferred in axial direction and how much is transferred in radial direction. Therefore two different HTCs will be calculated assuming two different driving forces for the heat flux in the wall. Method I uses T_{w1} and T_{w2} (see Figure 10 and 21a) and method II uses T_{w1} and T_{out} (see Figure 10 and 21a). The maximum HTC value is based on method I. By the maximum HTC it is assumed that all the heat from a higher position will transferred to the water. The minimum HTC value is based on method II. Here it is assumed that only heat is transferred in radial direction and is not influenced by the vertical heat flow. In reality the HTCs will probably be between this maximum and minimum value.

Figure 24 shows the maximum and minimum HTCs and the correlations with the different driving forces for the flow rate of 4 kg/h and a pressure of 300 bar. In this figure the maximum HTC lies much higher than the minimum HTC value, due to the higher temperature difference of T_{w1}-T_{w2} and higher corresponding heat flux. It is shown that the difference between the HTCs are large in the subcritical range. It was expected that that these HTCs are in the same order of magnitude and comparable with the HTCs at 55 cm, seen in Figure 15. The large difference can be explained by a maximum temperature in the wall. There is no explanation found for the maximum temperature in the wall at subcritical bulk temperatures.

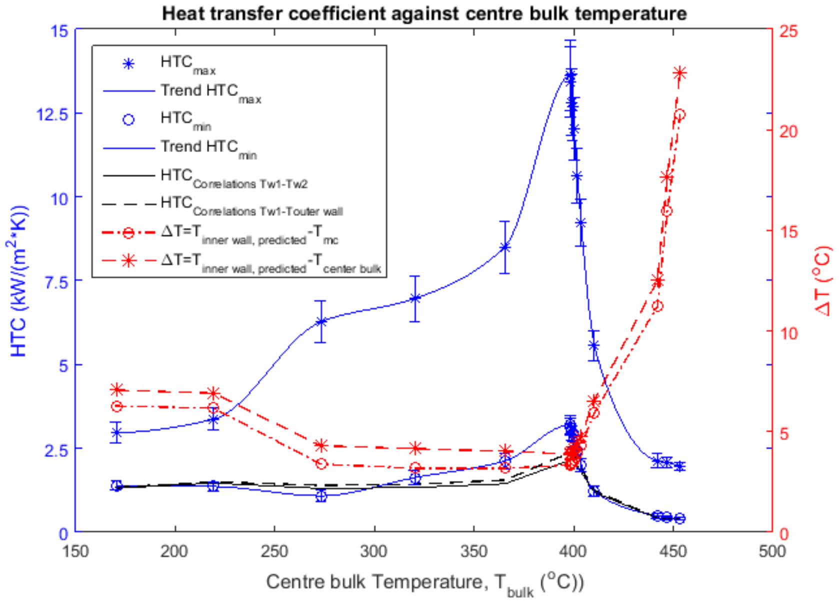

(a)

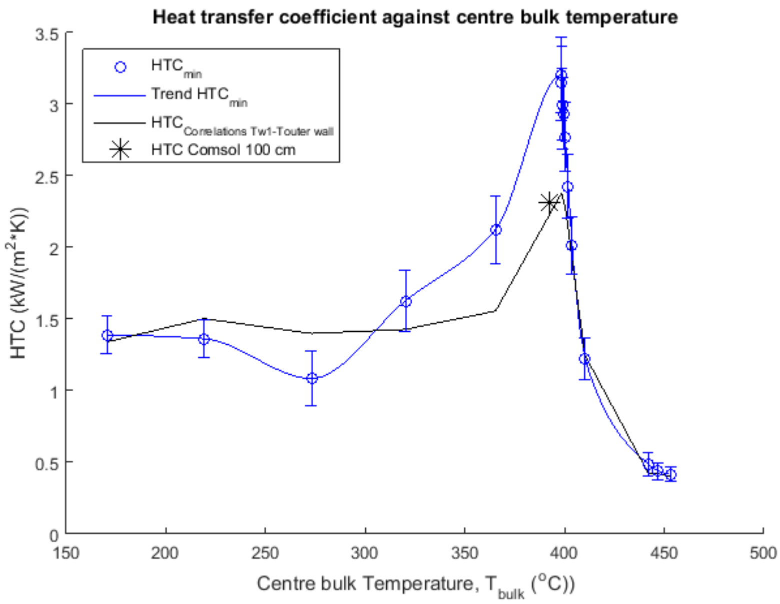

(b)

Figure 24: [a]: The maximum HTCs (blue star) and minimum HTCs (blue circle). The black lines are the HTCs based on the Nusselt correlation. The driving forces are plotted on the right y-axis. [b]: The minimum HTCs (blue circle line) and the HTCs based on the correlation (black line). The black star is the HTC result out Comsol simulations at 100 cm. Experimental parameters: H=100 cm, P=300 bar and φ_{water}=4 kg/h.

The way to predict the inner wall temperature is barely dependent on the method that is used (line I and II in Figure 21a. The driving forces are close to each other and therefore the HTCs from the correlation. In Figure 24(a) the solid black line is the HTC based on the temperature difference T_{w1}-T_{w2}. The banded black line is based on the temperature difference T_{w1}-T_{out}. Around the pseudocritical temperature the HTCs from the correlation are not showing a strange behaviour comparable to the results obtained at 55 cm, see Figure 15. This is due to the higher driving force at 100 cm.

The black star, in Figure 24(b), is the HTC at 100 cm from Comsol simulations. This result is close to the correlation and lower than the experimental value. During the simulations with Comsol a normal temperature profile in the wall was seen (no vertical heat transfer) and as seen in Figure 24(b) this result is close to the minimum experimental HTCs. Also the minimum HTCs at 100 cm are comparable to the experimental HTCs at 55 cm. Therefore it is likely that the minimum HTCs based on T_{w1} and T_{out}, without heat effects from higher tube sections, are correct.

Effect of flow rate

Next to the 4 kg/h also a flow rate of 8 kg/h is examined at the height of 100 cm, see Figure 25. This figure shows the maximum and minimum HTCs for the experiments and for the correlation. The calculation method for the maximum and minimum experimental HTC are the same as for the 4 kg/h. The maximum HTC is based on the temperature difference of T_{w1} and T_{w2} and the minimum HTC is based on the temperature difference of T_{w1} and T_{out}. Three points are in line at the centre bulk temperature of 400°C. Here the preheater setting is different but the center bulk temperature remains the same. The difference in results of the maximum and minimum HTCs are not that extreme as for the 4 kg/h at 100 cm, due to a higher heat withdrawal rate for 8 kg/h. The HTCs of the correlation at 8 kg/h lies between the experimental maximum and minimum HTCs. This can imply that heat from a higher and hotter section in the tube wall is transferred to the water. Also the correlation is now close to the valid range of mass flux given in Table 2 which can give a more accurate HTC value. This is not the case for the 4 kg/h because the corresponding mass flux is 3 kg/m^2s.

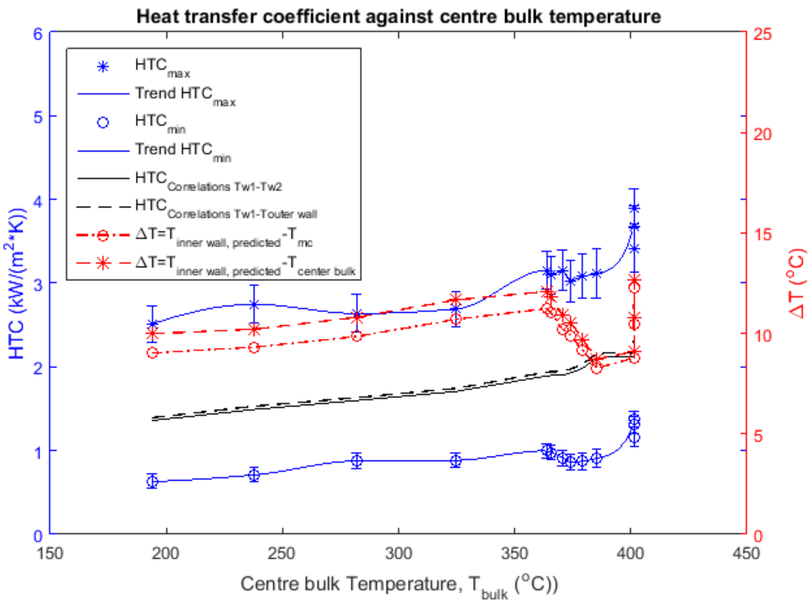

Figure 25: The maximum HTCs (blue star) and minimum HTCs (blue circle). The black lines are the HTCs based on the Nusselt correlation. The driving forces are plotted on the right y-axis. Experimental parameters: H=100 cm, P=300 bar and φ_{water}=8 kg/h.

Figure 26 shows the minimum experimental HTCs with the flow rate of 4 and 8 kg/h. In this figure the experimental HTCs of 4 kg/h lies above the 8 kg/h which is in contrast with the results at 55 cm and the literature. On the other hand the HTCs from the correlation at 8 kg/h is above the 4 kg/h, which is in line with the expectations.

Effect of pressure

The last experiments were done at a pressure of 250 bar, see Figure 27. This figure shows also the experimental maximum and minimum HTCs which have comparable trends as the 300 bar at 4 kg/h, see Figure 24a. This means that for the pressure of 250 bar there is also a maximum temperature in the wall, see Figure 29.

Figure 27 shows the experimental and the correlation minimum HTCs for 250 and 300 bar. In this figure the HTC peak of 250 bar is left to the peak of 300 bar, due to a lower pseudocritical temperature at 250 bar. When the pressure decreases in the supercritical region the specific isobaric heat capacity of water increases, see Figure 2. This makes it possible that the peak of the HTC increases with a decrease in pressure. Yamagata et al. and Swenson et al. saw that the

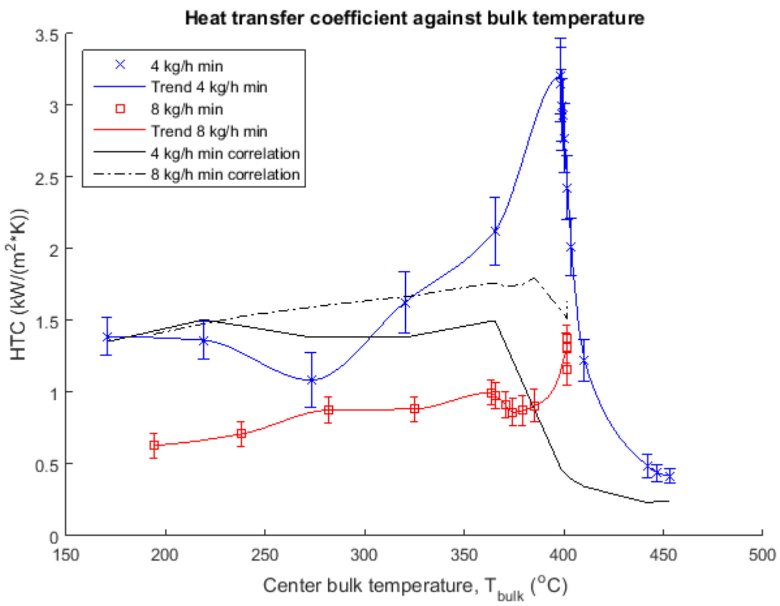

Figure 26: The minimum HTCs for i) 4 kg/h (blue) and ii) 8 kg/h (red). The black lines are the HTCs based on the Nusselt correlation. Experimental parameters: H=100 cm, P=300 bar.

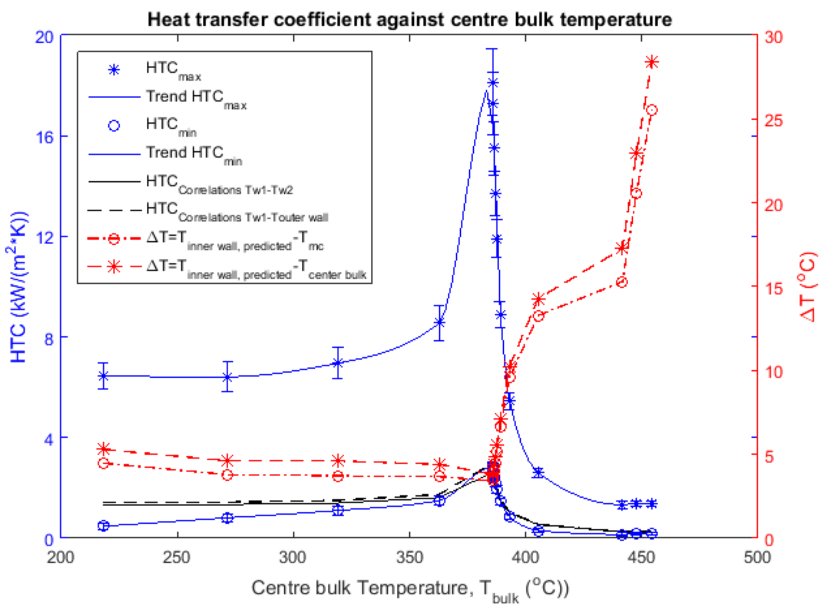

Figure 27: The maximum HTCs (blue star) and minimum HTCs (blue circle). The black lines are the HTCs based on the Nusselt correlation. The driving forces are plotted on the right y-axis. Experimental parameters: H=100 cm, P=250 bar and φ_{water}=4 kg/h.

HTC in the pseudocritical region becomes higher as the pressure approaches the critical pressure [16; 27]. In Figure 28 The HTCs are in the same order of magnitude at the centre bulk temperature around the 450°C. In Figure 29 radial temperature profiles are shown for the most right point of 250 and 300 bar. The difference in wall temperature cause the difference in HTC.

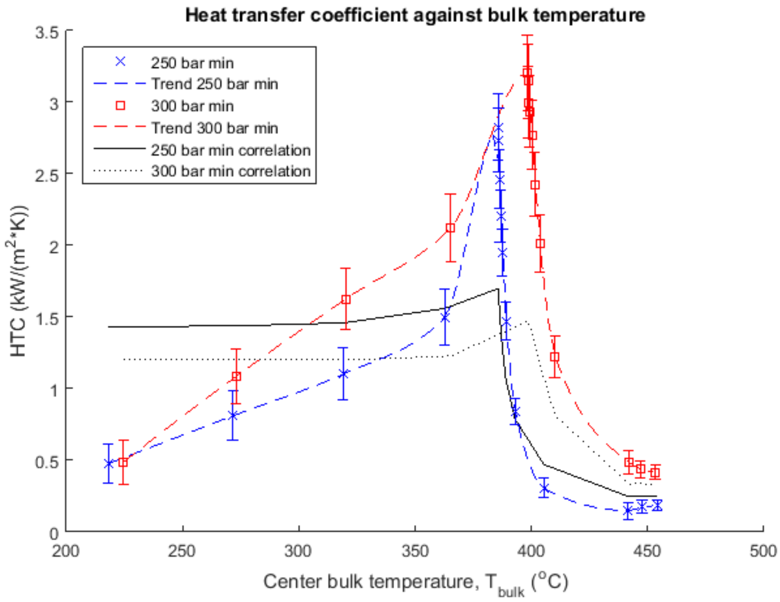

Figure 28: HTC of 250 bar (blue) and 300 bar (red) at flow rate of 4 kg/h, and H=100 cm.

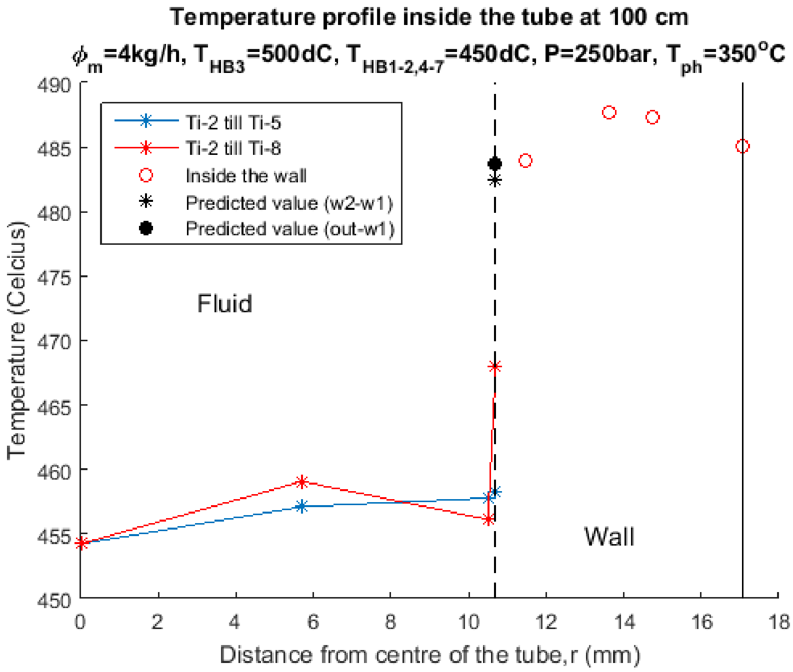

(a)

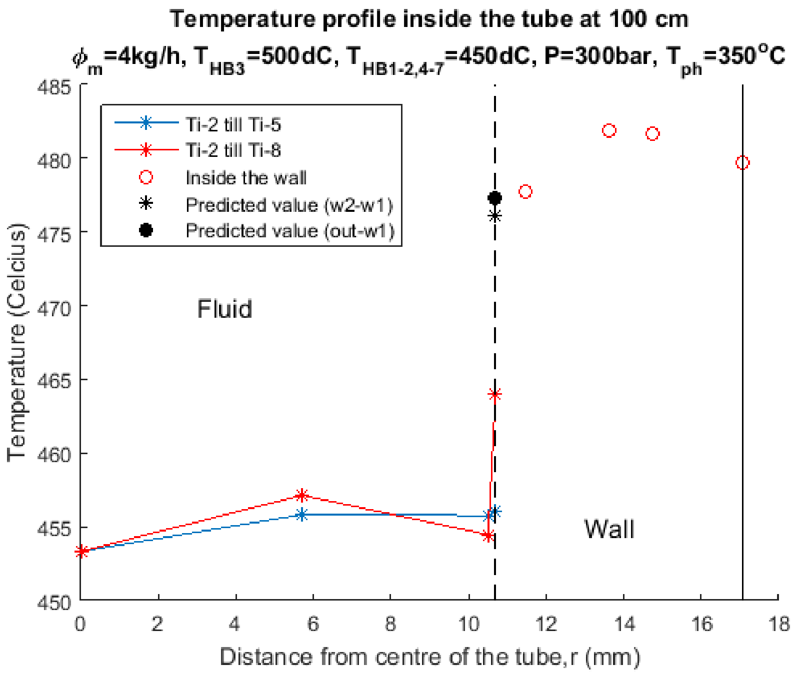

(b)

Figure 29: [a]: Supercritical radial temperature profile at H=100cm, P=250 bar and φ_{water}=4 kg/h. [b]: Supercritical radial temperature profile at H=100cm, P=300 bar and φ_{water}=4 kg/h.

5 Conclusions

In this research heat transfer experiments to sub- and supercritical water in a vertical heated tube are conducted to investigate the influence of different flow rates (4.1, 8.3 and 11.3 kg/h) and pressure levels (300 and 250 bar) on the heat transfer coefficient (HTC). Experiments were conducted at a height of 55 and 100 cm.

Experiments performed at 300 bar and a height of 55 cm show:

- In general a flat temperature profile in the water phase with a steep temperature increase close to the wall (within 0.2 mm from the wall). This is in agreement with Comsol model calculations.
- That the experimental HTC is almost linearly increasing from 1 kW/m^2.°C at a bulk temperature of 100°C up to 2 kW/m^2.°C at a bulk temperature of 350°C for all flows investigated.
- Above 350 °C the experimental HTC for 4.1 and 8.3 kg/h shows an exponential increase up to the pseudocritical temperature (400°C at 300 bar) after which it drops again for the 4.1 kg/h. At higher flow rates it is not possible to pass the 400 °C level due to a lack of heating power.
- The effect of flow rate is examined and there is an increase in HTC with increasing flow rate. This effect is also reported in literature.
- At subcritical temperature the HTCs calculated with the correlation fits to experimental HTCs within the error margin. In general the HTCs calculated with the correlation under predicts the experimental HTCs. When the bulk temperature comes closer to (pseudo-) critical temperature more deviation between the experimental and correlation HTCs is found. A strange behavior of the correlation is found around the pseudocritical temperature. The driving force (T_{wall}-T_{bulk}) becomes low which has a strong effect on the outcome of the correlation.

New experiments at 100 cm were performed because the maximum temperature was restricted by the power input below 55 cm at higher flow rates. Experiments at 100 cm give more heating power. The maximum value of the 4.1 kg/h is also found at this height but no maximum for 8.3 kg/h.

During the experiments, at a height of 100 cm, a strange phenomenon was detected: a maximum in the inner wall temperature. The hypothesis of a vertical heat flow in the tube wall is studied and most probable the reason for this temperature profile. It is unknown what exactly happens inside the tube wall in terms of heat transfer and how to distinguish between the radial and axial heat flux. This is essential to calculate the value of the HTCs. More experimental and simulation research is therefore needed.

The effect of pressure (250 and 300 bar) are clearly shown in the results. The HTCs are lower and the peak is at a lower bulk temperature when the pressure approached the critical pressure of water.

6 Recommendations

The experimental results and the results of the correlation deviate the most around the pseudocritical temperature. The correlation shows a strange u due to the small temperature difference between the wall and fluid at 55 cm. At larger temperature differences between the wall and fluid, as at the height of 100 cm, this behaviour is less pronounced. The correlation is thus sensitive for the temperature difference, which becomes small around the pseudocritical temperature. It is recommended to do more Comsol simulation in this temperature region and if necessary, make adjustment to the Nusselt correlation.

Investigate the influence of the experimental procedure on the experimental HTC results. In this research the temperature of the heating blocks is increased stepwise (at a preheater temperature of 20°C) and when the heating block temperature is maximal the temperature of the preheater is increased. The bulk temperature increased to the (pseudo-) critical temperature when the temperature of the preheater increased. The temperature difference and so the driving force become therefore smaller. The influence of this experimental procedure on the HTC is unknown. The reason is that the heat transfer from the wall to the fluid is larger when the temperature become close to the (pseudo-) critical temperature and therefore also the temperature difference become smaller. A change in sequence of increasing the temperature of the heating block and preheater can show whether or not the experimental procedure has influence on the HTC.

The experiments at 100 cm show a maximum in the wall temperature profile. The different calculation methods for the heat flux result in significant different results for the HTCs. This radial gradient is probably due to an axial temperature gradient in the wall. This should be avoided by adjusting the T-settings of the heating blocks to get a constant temperature profile around 100 cm.

Apply a different method to calculate the radial heat flux. The heat flux is now calculated based on the radial temperature gradient in the wall. An alternative is the heat flux calculation based on the change in temperature of the fluid. The temperature at the hart of the tube is measured for two axial positions, which are 5 cm apart. With these temperatures the change in enthalpy can be calculated and consequently the heat flux for this section.

7 Acknowledgement

First of all I would like to thank Professor Sascha Kersten for the opportunity to do my master thesis in his research group. My deepest and special thanks for Samual Odu MSc. to work on his subject on heat transfer of supercritical water. I found the collaboration very pleasant with Samuel. I would thank Samuel the feedback, knowledge and discussions on the subject. There were a lot of technical challenges where I would thank the technicians Johan Agterhorst and Benno Knaken for the quick repairs and discussions on technical problems. Also I want to thank dr. ir. Louis van der Ham and dr. ir. Wim Brilman for discussions and a critical look at my work. As last I would like to thank dr. ir. Martin van der Hoef for taking a place in my committee.

Finally I want to thank my family and girlfriend for supporting me during my study in the last 6.5 years.

8 Bibliography

[1] H. et. al. Weingartner. *Water, 1. Properties, Analysis and Hydrological Cycle.* Wiley-VCH Verlag GmbH & Co. KGaA, 2000. doi: 10.1002/14356007.a28_001.pub2.

[2] Y. et. al. Matsumura. Biomass gasification in near- and super-critical water: Status and prospects. *Biomass and Bioenergy*, 29(4):269–292, 2005. doi: http://dx.doi.org/10.1016/j.biombioe.2005.04.006.

[3] Sarah Mokry, Igor Pioro, Pavel Kirillov, and Yevgeniy Gospodinov. Supercritical-water heat transfer in a vertical bare tube. *Nuclear Engineering and Design*, 240(3):568–576, 2010. doi: http://dx.doi.org/10.1016/j.nucengdes.2009.09.003.

[4] Igor Leonardovich Pioro and Romney B Duffey. *Heat transfer and hydraulic resistance at supercritical pressures in power engineering applications.* American Society of Mechanical Engineers, 2007.

[5] R. Alaaedin and S.O. Odu. Heat transfer measurements for supercritical water flow in a vertical tube at low mass fluxes. Master's thesis, University of Twente, Enschede, 2015.

[6] P. Koster and S.O. Odu. Numerical analysis of heat transfer in supercritical water at low mass flux mixed convection conditions. Master's thesis, University of Twente, Enschede, 2014.

[7] Hannsjorg Freund and Kai Sundmacher. *Process Intensification, 2. Phase Level.* Wiley-VCH Verlag GmbH & Co. KGaA, 2000. doi: http://dx.doi.org/10.1002/14356007.o22_o03.

[8] Sarah Morky and Igor Pioro. *Thermophysical Properties at Critical and Supercritical Conditions*, chapter 22, pages 573–592. InTech, Oshawa, 2011.

[9] Nathan Oldridge. Phase diagrams, 2013.

[10] David J Dixon and Keith P Johnston. Supercritical fluids. *Kirk-Othmer Encyclopedia of Chemical Technology*, 1997.

[11] The EngineeringToolbox. Water - density and specific weight, August 2015. URL `http://www.engineeringtoolbox.com/water-density-specific-weight-d_595.html`.

[12] The Engineering Toolbox. Properties of saturated steam - pressure in bar. URL `http://www.engineeringtoolbox.com/saturated-steam-properties-d_457.html`.

[13] Magnus Holmgren. Xsteam: Water and steam properties according to iapws if-97. *www. x-eng. com*, 2007.

[14] X Cheng, T Schulenberg, S Koshizuka, Y Oka, and A Souyri. Thermal-hydraulic analysis of supercritical pressure light water reactors. 2002.

[15] Marc Hodes, Philip A. Marrone, Glenn T. Hong, Kenneth A. Smith, and Jefferson W. Tester. Salt precipitation and scale control in supercritical water oxidationâĂŤpart a: fundamentals and research. *The Journal of Supercritical Fluids*, 29(3):265 – 288, 2004. ISSN 0896-8446. doi: http://dx.doi.org/10.1016/S0896-8446(03)00093-7. URL `http://www.sciencedirect.com/science/article/pii/S0896844603000937`.

[16] K Yamagata, K Nishikawa, S Hasegawa, T Fujii, and S Yoshida. Forced convective heat transfer to supercritical water flowing in tubes. *International Journal of Heat and Mass Transfer*, 15(12):2575–2593, 1972.

[17] Chaobin Dang and Eiji Hihara. In-tube cooling heat transfer of supercritical carbon dioxide. part 1. experimental measurement. *International journal of refrigeration*, 27(7):736–747, 2004.

[18] J Fewster and JD Jackson. Experiments on supercritical pressure convective heat transfer having relevance to spwr. Technical report, American Nuclear Society, 555 North Kensington Avenue, La Grange Park, IL 60526 (United States), 2004.

[19] RA Lee and KH Haller. Supercritical water heat transfer developments and applications. In *Proceedings of the 5th International Heat Transfer Conference, Tokyo, Japan, September*, pages 3–7, 1974.

[20] AA Bishop, RO Sandberg, and LS Tong. Forced-convection heat transfer to water at near-critical temperatures and supercritical pressures. Technical report, Westinghouse Electric Corp., Pittsburgh, Pa. Atomic Power Div., 1964.

[21] S.O. Odu, P. Koster, A.G.J. van der Ham, M.A. van der Hoef, and S.R.A. Kersten. Heat transfer to sub- and supercritical water at low mass fluxes: Numerical analysis and experimental validation. 2015.

[22] V.A. Kurganov. Heat transfer coefficient, February 2011.

[23] Abraham Tamir and Yehuda Taitel. On the concept of the "mixing cup" temperature in flows with axial conduction. *The Canadian Journal of Chemical Engineering*, 50(3):421–424, 1972. ISSN 1939-019X. doi: 10.1002/cjce.5450500320. URL `http://dx.doi.org/10.1002/cjce.5450500320`.

[24] A. Bejan. *Convection Heat Transfer*. Wiley, 2013. URL `https://books.google.nl/books?id=9yC91-gpU8sC`.

[25] J.G. Hust and P. J. Giarratano. *Thermal Conductivity and Electrical Resistivity Standard Reference Materials: Austenitic Stainless Steel, SRM's 735 and 798, from 4 to 1200 K*, volume 260-46 of *Standard Reference Materials*. U.S. Department of Commerce, National Bureau of Standards, Boulder, Colorado, 1975.

[26] G Scalabrin, L Piazza, and M Condosta. Convective cooling of supercritical carbon dioxide inside tubes: heat transfer analysis through neural networks. *International journal of heat and mass transfer*, 46(23):4413–4425, 2003.

[27] HS Swenson, JR Carver, and CR d Kakarala. Heat transfer to supercritical water in smooth-bore tubes. *Journal of Heat Transfer*, 87(4):477–483, 1965.

[28] et al. Meulen, J.v.d. *Algemene Practicumhandleiding*. University of Twente, Faculty of Science and Technology, 2009.

[29] H.J.C. Berendsen. *Goed meten met fouten*. Rijksuniversiteit Groningen, 2009.

Appendix I: Thermocouples configuration

Thermocouples to measure temperatures inside the HEX at 55 cm

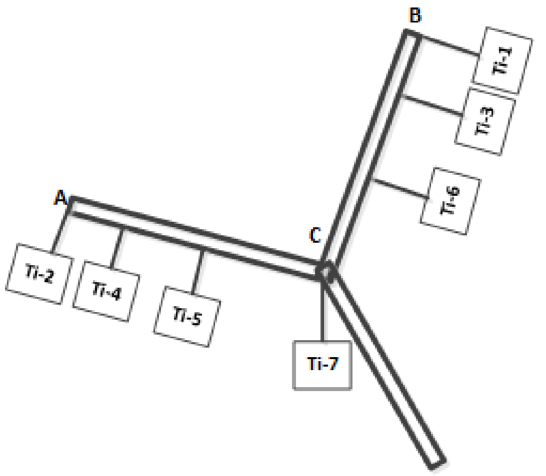

A –> C = B -> C = IR = 10.7 mm

Ti1/Ti2 =touching the wall

Ti3 = 0.2 mm from B (the inner wall)

Ti4 = 0.2 mm from A (the inner wall)

Ti5 = 5 mm from A (the inner wall)

Ti6 = 5 mm from B (the inner wall)

Ti7 = at center of tube

Thermocouples to measure outside wall temperatures

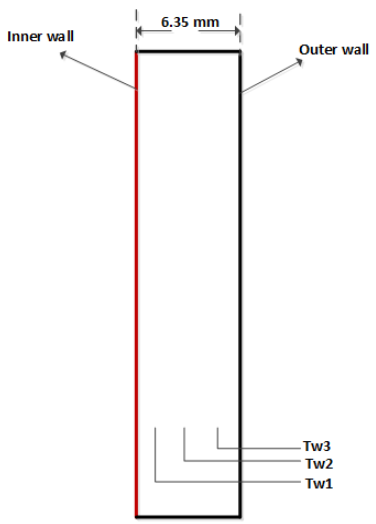

Thermocouples welded to the wall

Outer wall Temp. Probe	Position -> from bottom (cm)
T1-HB1 top	150
T2-HB1 bottom	136
T3-HB2 top	128
T4-HB2 bottom	114
T5-HB3 top	106
T6-HB3 bottom	92
T7-HB4 top	84
T8-HB4 bottom	70
T9-HB5 top	62
T10-HB5 middle	55
T11-HB5 bottom	48
T12-HB6 top	40
T13-HB6 middle	33
T14-HB6 bottom	26
T15-HB7 top	18
T16-HB7 middle	11
T17-HB7 bottom	4

Position inside tube wall at axial positions: 11 cm, 33 cm, 55 cm

Tw1	1 mm from inner wall = 5.35 mm from outer wall
Tw2	3 mm from inner wall = 3.35 mm from outer wall
Tw3	5 mm from inner wall = 1.35 mm from outer wall

Thermocouples to measure temperatures inside the HEX at 100 cm

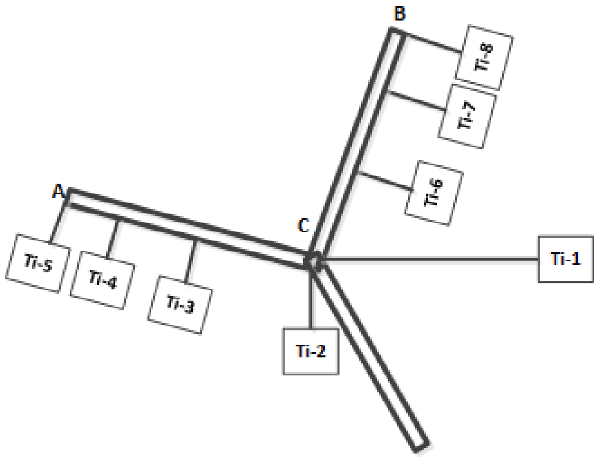

A –> C = B -> C = IR = 10.7 mm

Ti1 = at center of tube, low position

Ti2 = at center of tube, high position

Ti3 = 5 mm from A (the inner wall)

Ti4 = 0.2 mm from A (the inner wall)

Ti5 = against the inner wall

Ti6 = 5 mm from B (the inner wall)

Ti7 = 0.2 mm from B (the inner wall)

Ti8 = against the inner wall

Thermocouples to measure outside wall temperatures

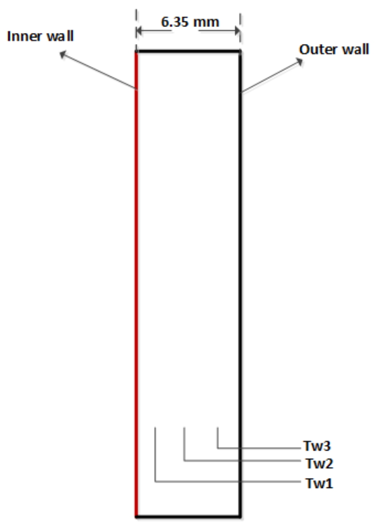

Thermocouples welded to the wall

Outer wall Temp. Probe	Position -> from bottom (cm)
T1-HB1 top	150
T2-HB1 bottom	136
T3-HB2 top	128
T4-HB2 bottom	114
T5-HB3 top	106
T--HB3 middle	100
T6-HB3 bottom	92
T7-HB4 top	84
T8-HB4 bottom	70
T9-HB5 top	62
T10-HB5 middle	55
T11-HB5 bottom	48
T12-HB6 top	40
T13-HB6 middle	33
T14-HB6 bottom	26
T15-HB7 top	18
T16-HB7 middle	11
T17-HB7 bottom	4

Position inside tube wall at axial positions: 11 cm, 33 cm, 55 cm

Tw1	1 mm from inner wall = 5.35 mm from outer wall
Tw2	3 mm from inner wall = 3.35 mm from outer wall
Tw3	5 mm from inner wall = 1.35 mm from outer wall

Position inside tube wall at axial position: 100 cm

Tw1	0.75 mm from inner wall = 5.60 mm from outer wall
Tw2	2.94 mm from inner wall = 3.41 mm from outer wall
Tw3	3.95 mm from inner wall = 2.30 mm from outer wall

Appendix II: Results of a pressures of 230 bar at a height of 55cm

At the measured height of 55 cm experiments at a pressure of 230 bar were done with heating block temperature of 400°C, a preheater temperature range of 20-350°C and flow rates of 8 and 11.34 kg/h. The results are shown in this Appendix.

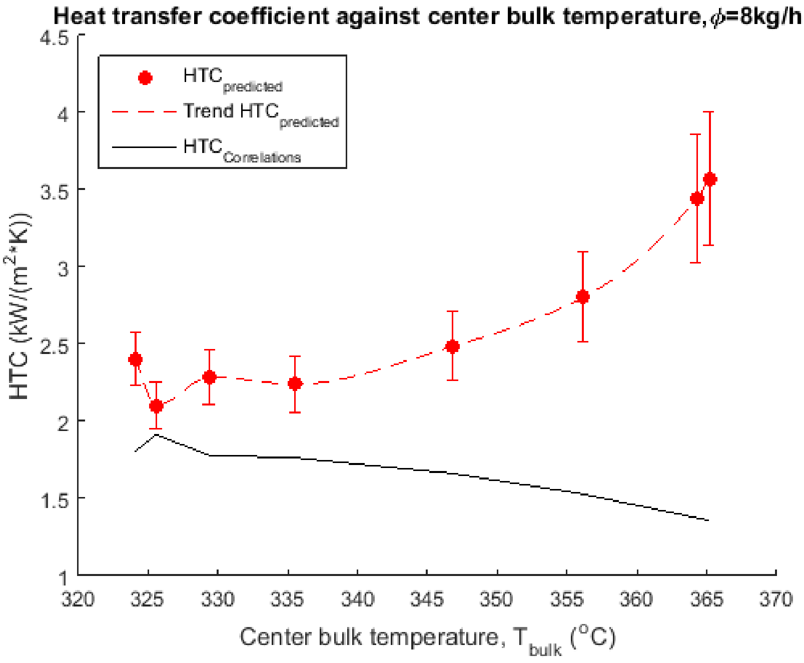

Figure 30: HTCs with a flow rate of 8 kg/h at 230 bar and a height of 55 cm.

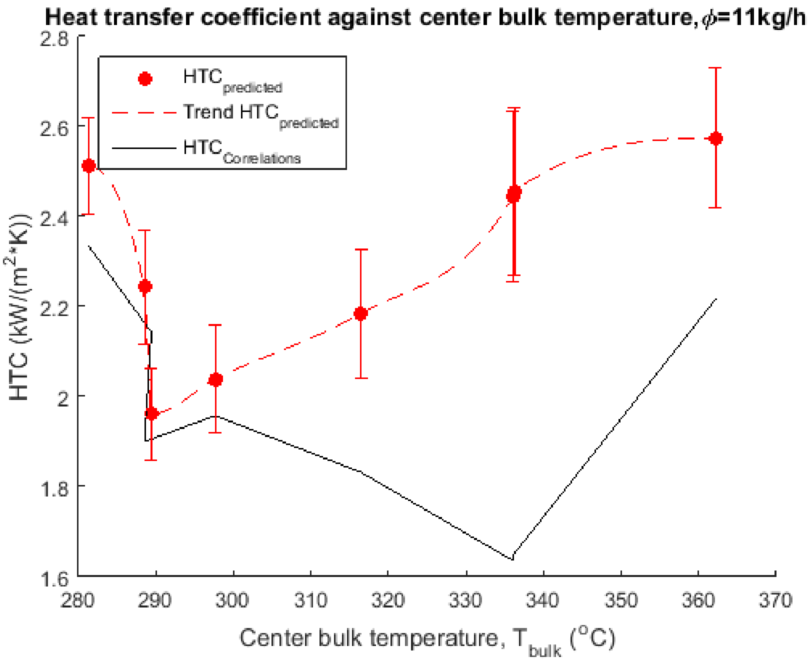

Figure 31: HTCs with a flow rate of 11 kg/h at 230 bar and a height of 55 cm.

Appendix III: Explanation radial temperature profiles

In chapter Results a higher inside wall temperature than the outer wall temperature was shown. In this chapter the reason is given that there is a strong change in heat transfer coefficient at the point the measurement is taken. Where below the critical temperature a good heat transfer is from the wall to the water and the heat transfer at the critical temperature is good. If the temperature is higher than the critical temperature the heat transfer become bad. That means that the heat supplied above the critical temperature is not transferred fast enough to the supercritical water. Below the critical temperature there is strong heat transport in radial direction and therefore also a lower wall temperature. The energy is now transported in vertical direction from the hotter wall section to the colder wall section when the temperature is higher than the critical temperature. This is now more dominant because the radial transport has dropped. In this appendix several points will be check from experimental data to support this hypothesis.

The different points to support this hypothesis are:

1. What is the temperature above the measured height?
2. How looks the radial temperature profiles with a temperature lower than 300°C?
3. What is the influence of a lower setting temperature of HB2 (HB2 is higher than HB3, HB3 is at measured position)?

The results are shown in the tables below. First some information about the outline of the tables and some comments on the figures.

The outline of the figures with a supercritical fluid:

Table 3: Supercritical fluids outline.

100 cm, new thermocouples	100 cm, old thermocouples
99 cm	55 cm

For the subcritical fluid is the outline:

Table 4: Subcritical fluids outline.

4 kg/h, $T_{HB,measured,heigth}$=200°C	4 kg/h, $T_{HB,measured,heigth}$=250°C
8 kg/h, $T_{HB,measured,heigth}$=200°C	8 kg/h, $T_{HB,measured,heigth}$=250°C
11 kg/h, $T_{HB,measured,heigth}$=200°C	11 kg/h, $T_{HB,measured,heigth}$=250°C

There are some comments on the figures, namely:

- The figure in the left upper corner by supercritical water; all the thermocouples are from the same batch. The thermocouples in the wall are replaced with new ones, but in the fluid there are old ones (in terms of operating time).
- Temperature results, in the figure in the left upper corner, of Ti-8 is not plotted in this figure because it was broken.
- The thermocouples which do the measurement on the wall temperature in the case of 99 cm and 100 cm are at the same positions/height.
- Outer wall temperature of bottom heating block 2, top heating block 3 and bottom heating block 3 and are added to the radial temperature profile plots. Discussion of the results.

Discussion of the results

The results of the first point of supporting the hypothesis are shown in Figure 32-34. These tables shown a higher temperature of HB3-top and HB2-Bottom compared to HB3-middle; the measured height (except for the 11 kg/h, H=99 cm). This makes the hypothesis possible that heat is transferred from a higher and hotter position to a lower and cooler position. Also by an increasing flow there is an increasing driving force from the wall to the fluid. Therefore there is a higher driving forces and so an increasing heat flux and a better heat transfer in radial direction. This is also can be seen by an increasing flux where a decreasing temperature peak in the wall occurs.

In Figure 36-37 radial temperature profiles with a temperature of heating block of the measured height is 200°C or 250°C. Here the expected temperature profile is shown where there is no influence of the heat in a higher location. So in that case of subcritical circumstances there is no vertical heat transfer in the wall of the tube.

For the third and last point results with a setting temperature of heating block 3 of 485°C and 500°C are shown in Figure 35. Heating blocks 1-2 and 4-7 were set on 450°C. In this table still the temperature gradient in the wall is shown, because the temperature of the top position of heating block 3 is higher than the middle position. So there is no uniform heating within the heating block and there is vertical heat transfer within one heating block section.

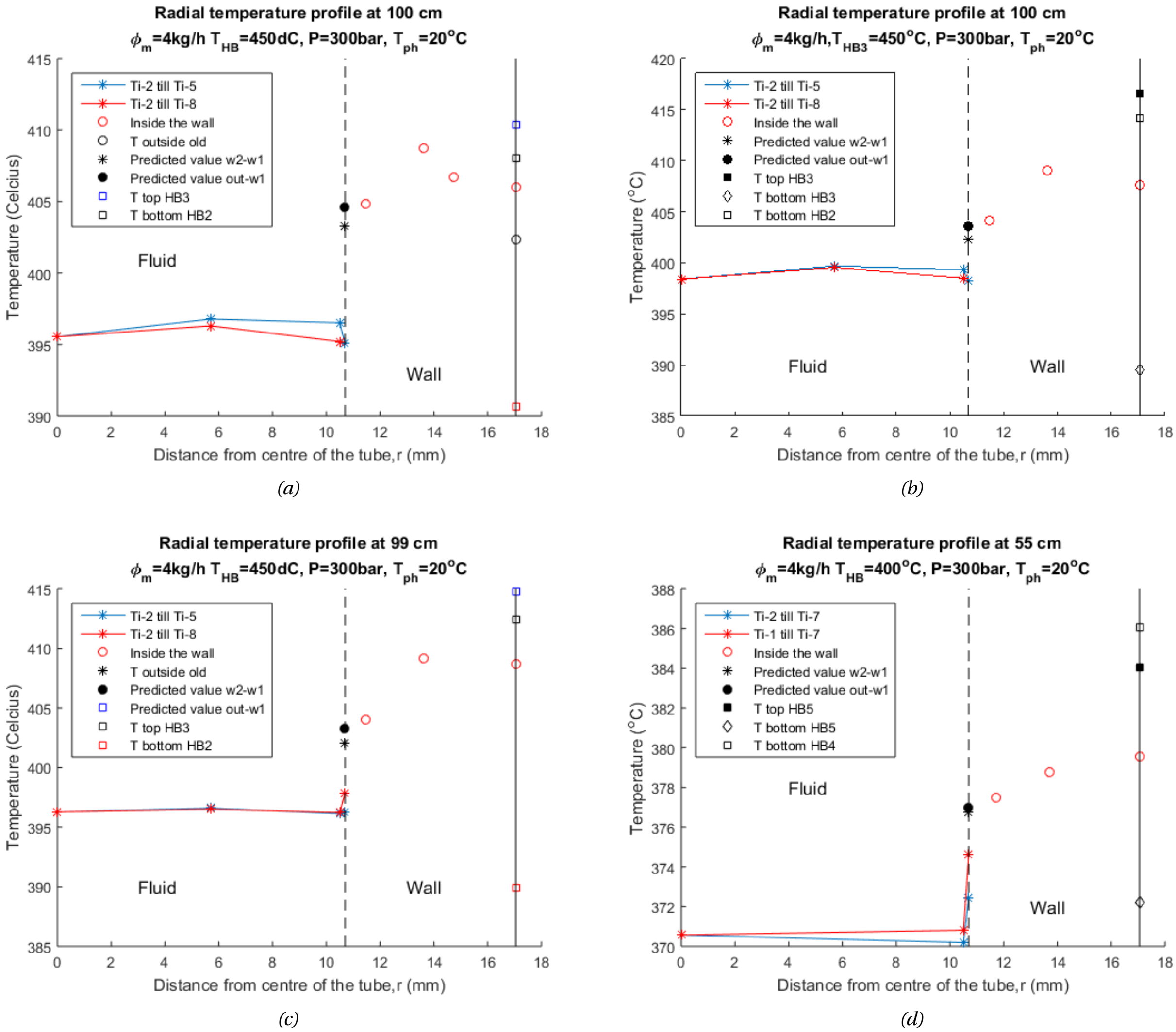

Figure 32: Radial temperature profile of 4 kg/h at supercritical conditions. (a) new thermocouples in the wall, (b) old thermocouples in the wall, (c) old thermocouples in the wall and (d) thermocouples in the wall are from an other batch.

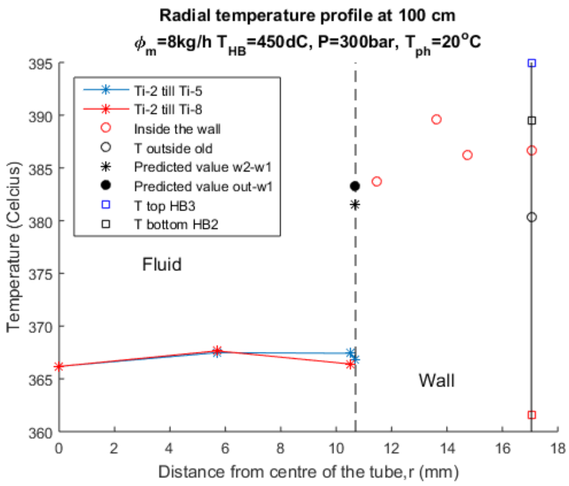

(a)

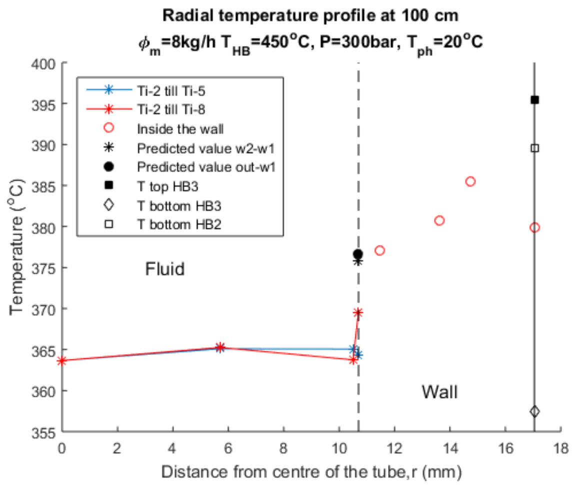

(b)

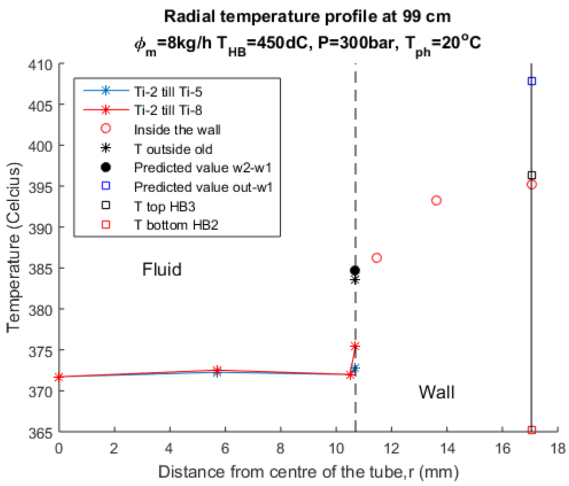

(c)

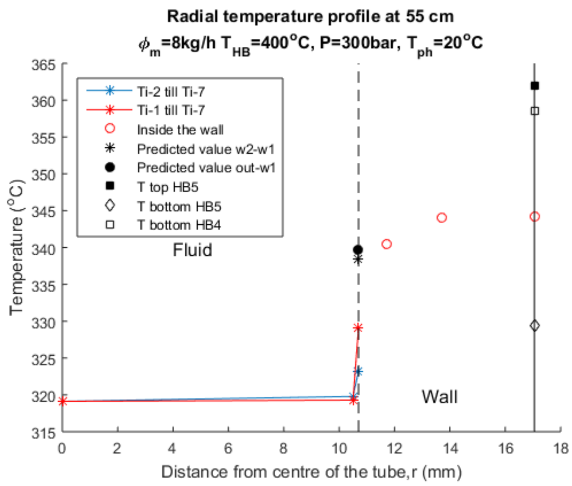

(d)

Figure 33: Radial temperature profile of 8 kg/h at supercritical conditions. (a) new thermocouples in the wall, (b) old thermocouples in the wall, (c) old thermocouples in the wall and (d) thermocouples in the wall are from an other batch.

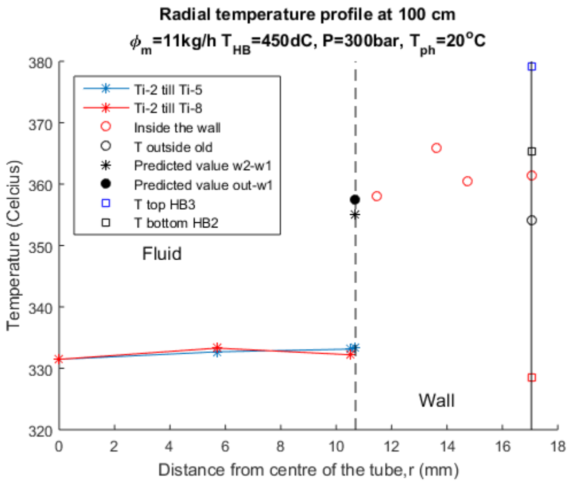

(a)

There are no experiments done for 11 kg/h in this situation

(b)

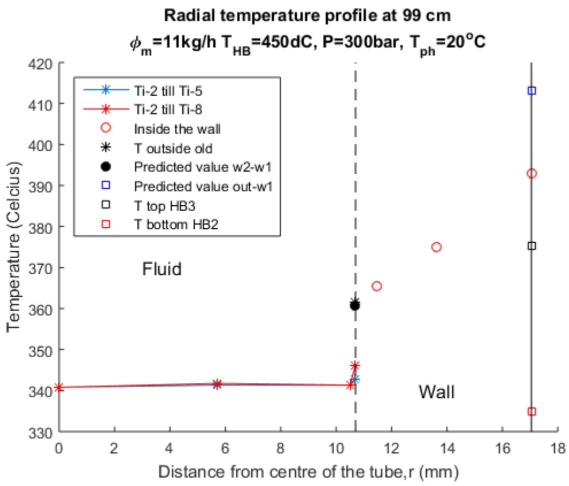

(c)

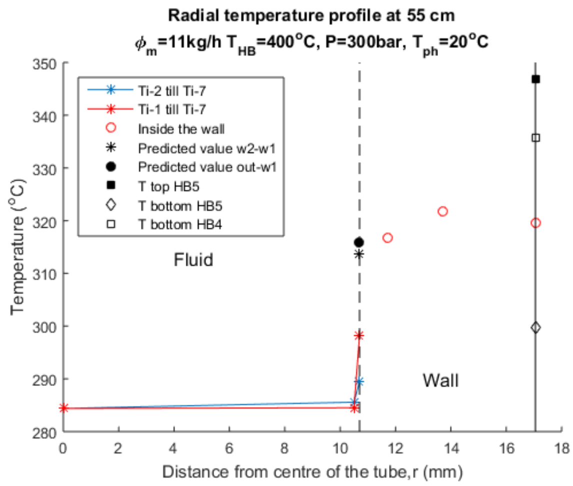

(d)

Figure 34: Radial temperature profile of 11 kg/h at supercritical conditions. (a) new thermocouples in the wall, (b) old thermocouples in the wall, (c) old thermocouples in the wall and (d) thermocouples in the wall are from an other batch.

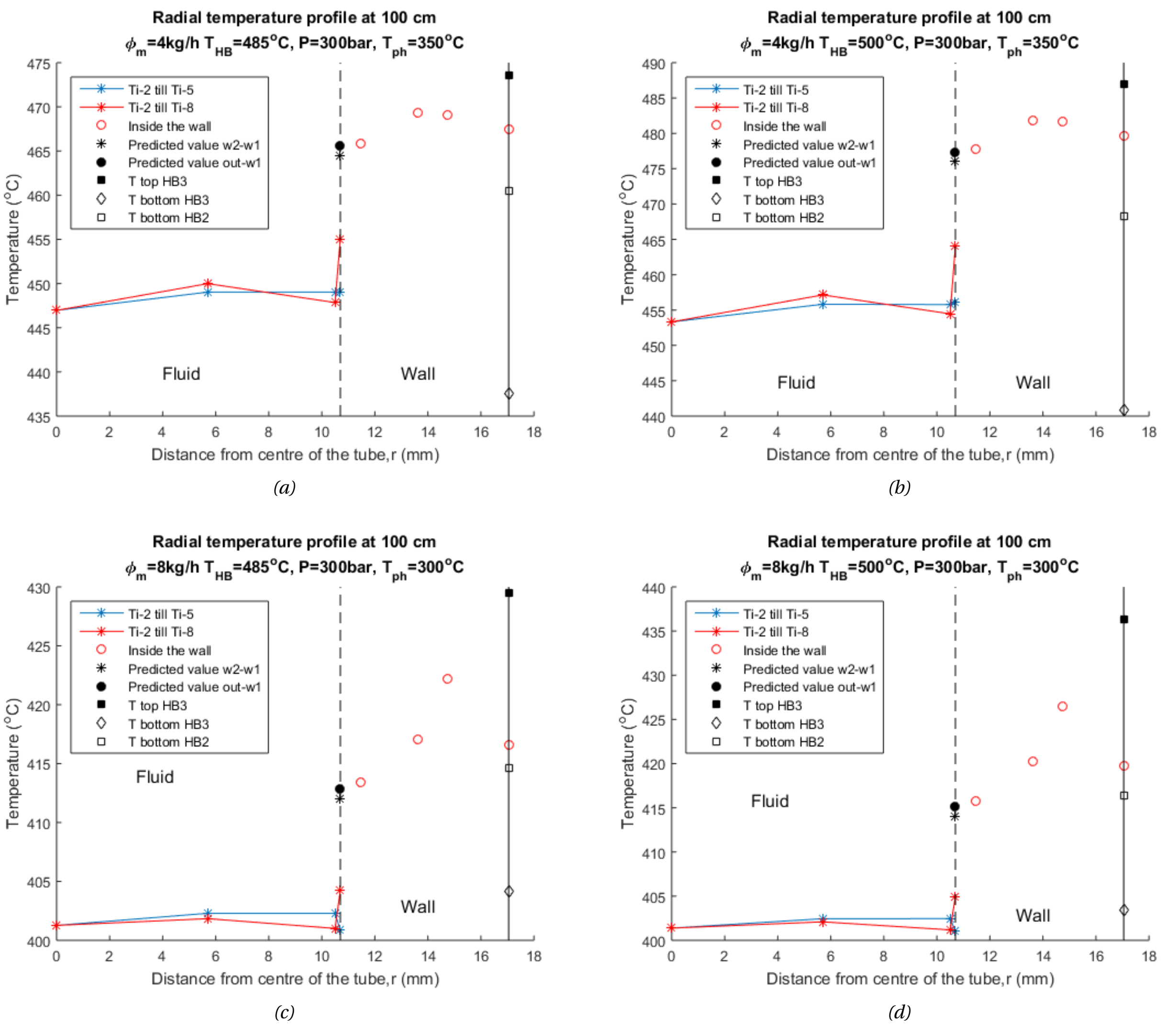

Figure 35: Radial temperature profile with a T_{HB2}<T_{HB3}. In all figures the thermocouples in the wall are from the same batch.

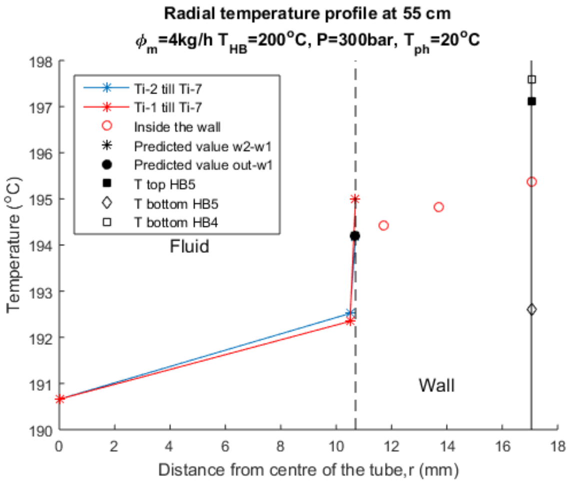

(a)

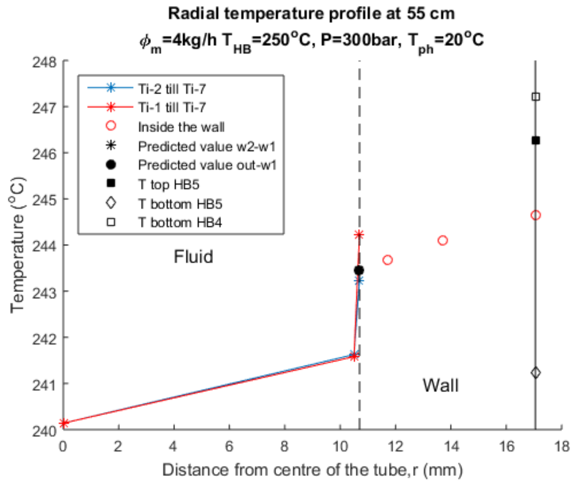

(b)

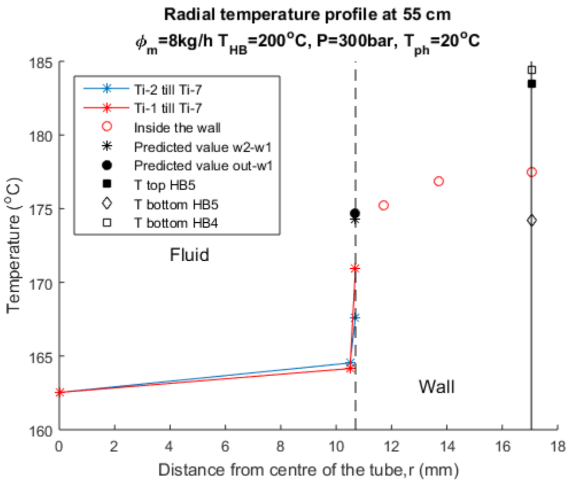

(c)

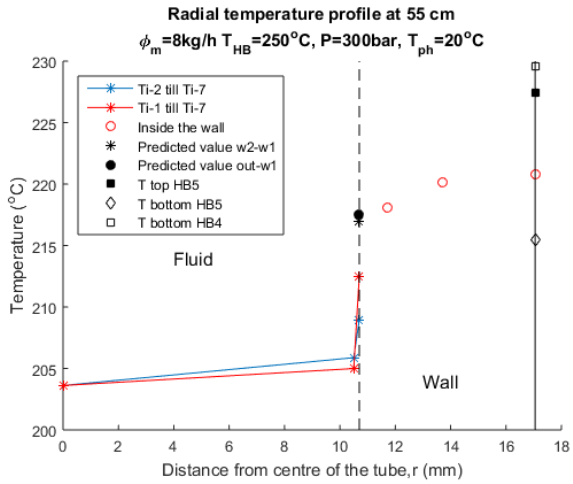

(d)

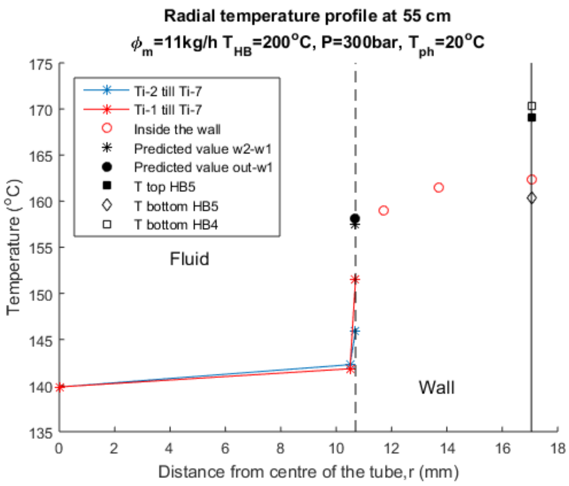

(e)

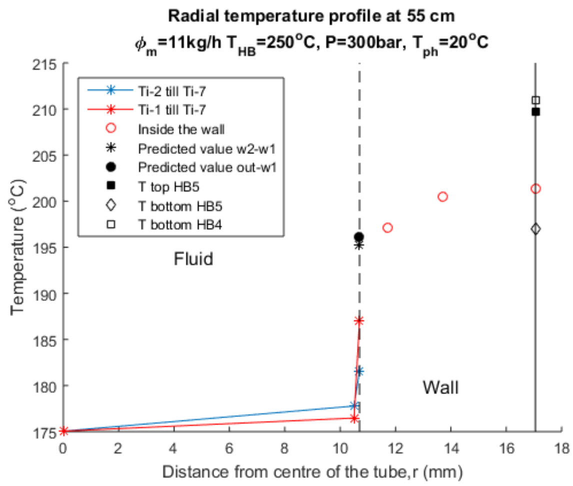

(f)

Figure 36: Radial temperature profile at 55 cm at low temperate (subcritical phase) for 4 (above), 8 (middle) and 11 kg/h (under) with heating block on 200^o C (left) and 250^o C (right).

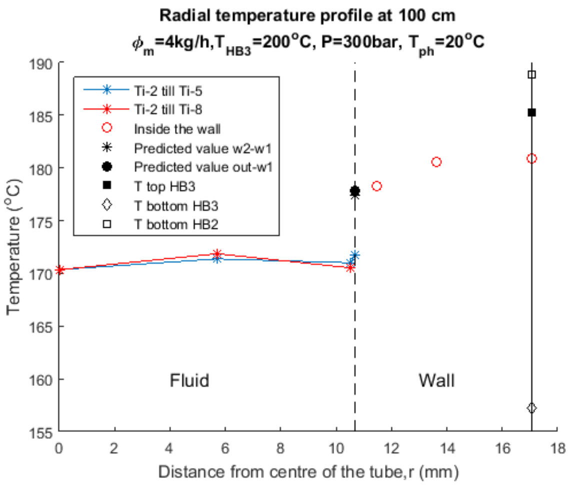

(a)

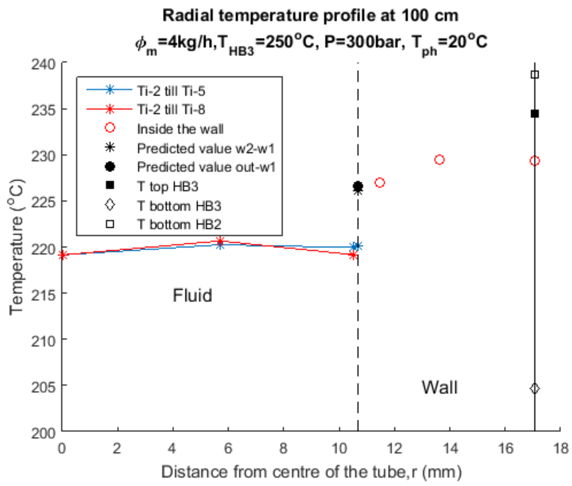

(b)

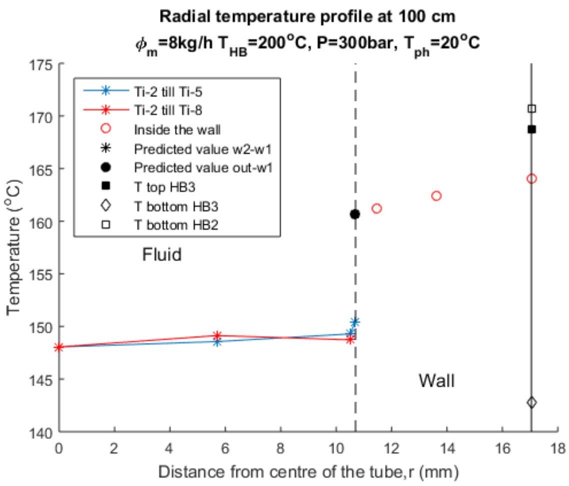

(c)

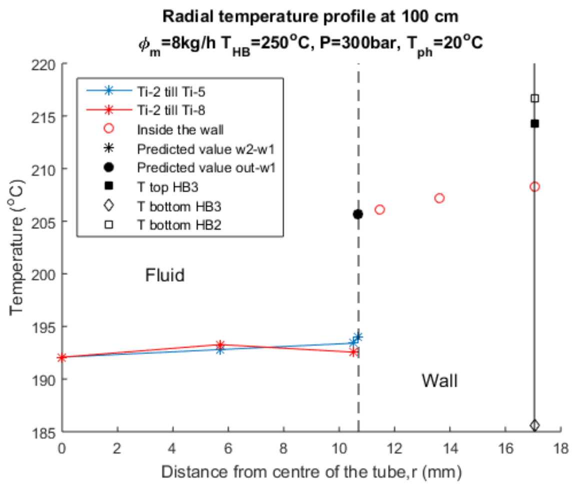

(d)

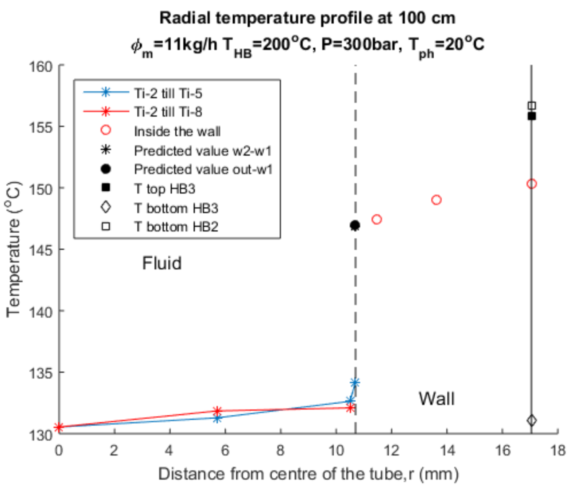

(e)

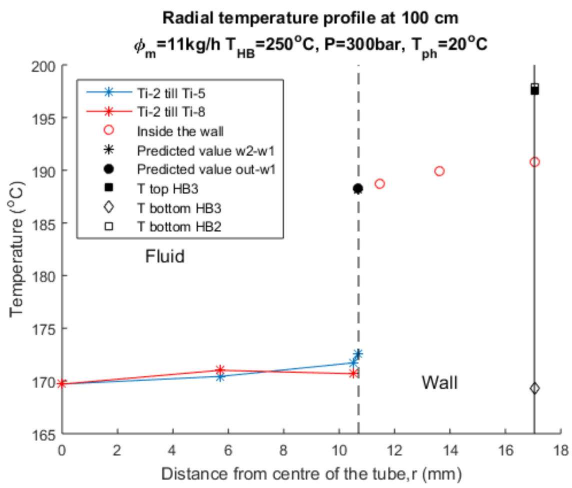

(f)

Figure 37: Radial temperature profile at 100 cm at low temperate (subcritical phase) for 4 (above), 8 (middle) and 11 kg/h (under) with heating block on 200^0 C (left) and 250^0 C (right).

Appendix IV: Error calculations

Temperature calculation:

$$T_{inner wall,prediction} = T_{w1} - \left(\frac{\ln\left(\frac{r}{r_1}\right)}{\ln\left(\frac{r_2}{r_1}\right)} * (T_{w1} - T_{w2}) \right) \tag{22}$$

Heat flux:

$$q'' = -k * \frac{T_{w1} - T_{w2}}{r * \ln\left(\frac{r_2}{r_1}\right)} \tag{23}$$

Thermal conductivity:

$$k = a * T_{inner wall}^{b} \tag{24}$$

HTC:

$$HTC = \frac{q''}{T_{wall} - T_{fluid}} \tag{25}$$

The absolute error in the Type-K thermocouples is experimentally determined. Four thermocouples were placed in a copper heating block for uniform heating. Three thermocouples, which were taken from the setup, have already been subjected to high temperatures during previous experiments. These three thermocouples are from the same batch and the fourth thermocouple is from a new batch without any high treatment. The temperature of the copper heating block was set at 300°C. When steady state was reached, temperature measurements of these thermocouples were recorded for 4 minutes.

In Figure 38 shows the temperature measurement over time. The fluctuations in temperature over time is due to the temperature control of the heating block. These fluctuations are the same for all four thermocouples, therefore the results were averaged for each thermocouple. The average of the three old thermocouples (from the setup and the same batch) is 303.58°C and the absolute error is ±0.10°C.

A correction factor of 2.30°C is added to the average temperature of the new thermocouple. This correction factor is found experimentally in a steady state surroundings. In this experiment different thermocouples of two batches are placed in water and heated till 90°C and had a temperature difference of 2.30°C. The average temperature of the fourth thermocouple is (after adding the correction factor) 303.36°C. The average temperature of all four thermocouples (old and new together) is 303.52°C. With this average temperature an absolute error of ±0.15°C is obtained.

For the position of the thermocouple, radius r, is measured with a Vernier Calliper and therefore the (possible) error is ±0.05 mm.

The error equations are made according to the 'Algemene Practicumhandleiding' of the faculty of Science and Technology of the University of Twente [28].

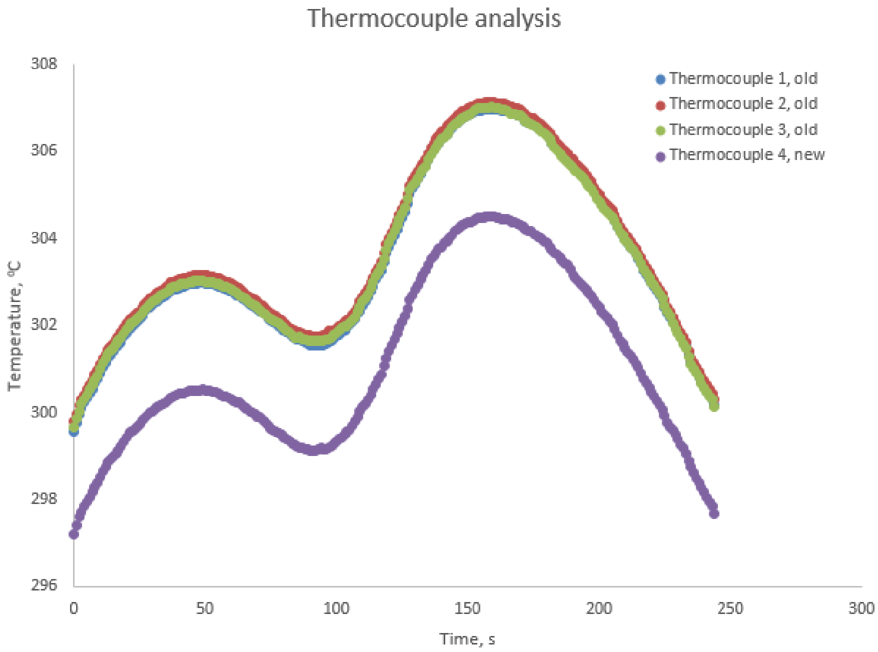

Figure 38: Thermocouple analysis for four different thermocouples. Experimental conditions: temperature copper heating block: 300°C and atmospheric pressure.

Temperature prediction

Error calculation in term:

$$d\ln(x) = d\ln\left(\frac{r}{r_1}\right) = \left(\frac{dr}{r} + \frac{dr}{r_1}\right) \tag{26}$$

$$d\ln(y) = d\ln\left(\frac{r_2}{r_1}\right) = \left(\frac{dr}{r_2} + \frac{dr}{r_1}\right) \tag{27}$$

Error calculation ln / ln-term

$$d\ln(total) = \frac{\ln\left(\frac{r}{r_1}\right)}{\ln\left(\frac{r_2}{r_1}\right)} * \left(\frac{d\ln(x)}{\ln\left(\frac{r}{r_1}\right)} + \frac{d\ln(y)}{\ln\left(\frac{r_2}{r_1}\right)}\right) \tag{28}$$

Error in $\left(\frac{\ln\left(\frac{r}{r_1}\right)}{\ln\left(\frac{r_2}{r_1}\right)} * (T_{w1} - T_{w2})\right) = A$:

$$dA = \frac{\ln\left(\frac{r}{r_1}\right)}{\ln\left(\frac{r_2}{r_1}\right)} * (T_{w1} - T_{w2}) * \sqrt{\left(\frac{\frac{2}{3} * d\ln(total)}{\frac{\ln\left(\frac{r}{r_1}\right)}{\ln\left(\frac{r_2}{r_1}\right)}}\right)^2 + \frac{dT^2 + dT^2}{(T_{w1} - T_{w2})^2}} \tag{29}$$

Error in temperature prediction:

$$dTr = \sqrt{dA^2 + dT^2} \tag{30}$$

Heat flux

Error in $r * \ln\left(\frac{r_2}{r_1}\right) = B$:

$$dB = r * \ln\left(\frac{r_2}{r_1}\right) * \left(\frac{d\ln(y)}{\ln\left(\frac{r_2}{r_1}\right)} + \frac{dr}{r}\right) \tag{31}$$

Error in $\frac{T_{w1}-T_{w2}}{r*\ln\left(\frac{r_2}{r_1}\right)} = C$:

$$dC = \frac{T_{w1} - T_{w2}}{r * \ln\left(\frac{r_2}{r_1}\right)} * \sqrt{\frac{2 * dT^2}{(T_{w1} - T_{w2})^2} + \left(\frac{\frac{2}{3} * dB}{r * \ln\left(\frac{r_2}{r_1}\right)}\right)^2} \tag{32}$$

Error in thermal conductivity

$$dk = |a| * T^b * |b| * \frac{dT}{T} \tag{33}$$

Error in heat flux:

$$dq = q * \sqrt{\left(\frac{dk}{k}\right)^2 + \left(\frac{dC}{\frac{T_{w1}-T_{w2}}{r*\ln\left(\frac{r_2}{r_1}\right)}}\right)^2} \tag{34}$$

HTC

$$dHTC = HTC * \sqrt{\frac{2 * dT^2}{(T_{w1} - T_{w2})^2} + \left(\frac{dq}{q}\right)^2} \tag{35}$$